

# **On the Thermal and Electrical Properties of Low Concentrator Photovoltaic Systems**

**Jacques Dewald Gerber**

Submitted in fulfilment of the requirements for the degree

***Magister Scientiae***

In the Faculty of Science at the  
Nelson Mandela Metropolitan University

December 2012

Supervisor: Prof EE van Dyk

Co-Supervisor: Dr FJ Vorster

## Declaration

Full names: Jacques Dewald Gerber

Student Number: 207032458

Qualification: Magister Scientiae

In accordance with Rule G4.6.3, I hereby declare that the above-mentioned treatise/dissertation/thesis is my own work and that it has not previously been submitted for assessment to another University or for another qualification.

A handwritten signature in black ink, appearing to read 'Jacques Dewald Gerber', written over a light blue grid background.

Jacques Dewald Gerber

7 December 2012

# **On the Thermal and Electrical Properties of Low Concentrator Photovoltaic Systems**

**Jacques Dewald Gerber**

Nelson Mandela Metropolitan University

The financial assistance of the National Research Foundation (NRF) towards this research is hereby acknowledged. Opinions expressed and conclusions arrived at, are those of the author and are not necessarily to be attributed to the NRF.

## ***ABSTRACT***

Low concentrator photovoltaic systems are capable of increasing the power produced by conventional silicon photovoltaic cells, thus effectively lowering the cost per kWh. However, power losses associated with resistance and temperature have limited the large scale implementation of this technology. In this study, the optical-, electrical- and thermal sub-systems of a low concentrator photovoltaic system are theoretically and experimentally evaluated with the aim of minimizing the power losses associated with series resistance and temperature. A 7-facet reflector system, with an effective concentration ratio of 4.7, is used to focus irradiance along a string of series connected poly-crystalline photovoltaic cells. I-V characteristics of 4-, 6- and 8-cell photovoltaic receivers are measured under 1-sun and 4.83-sun conditions. Under concentration, the 8-cell photovoltaic receiver produced 23% more power than the 4-cell photovoltaic receiver, which suggests that the effect of series resistance can be minimized if smaller, lower current photovoltaic cells are used. A thermal model, which may be used to predict operating temperatures of a low concentrator photovoltaic system, is experimentally evaluated within a thermally insulated enclosure. The temperatures predicted by the thermal model are generally within 5% of the experimental temperatures. The high operating temperatures associated with the low concentrator photovoltaic system are significantly reduced by the addition of aluminium heat sink. In addition, the results of a thermal stress test indicated that these high operating temperatures do not degrade the photovoltaic cells used in this study. The results of this study suggest that the power output of low concentrator photovoltaic systems can be maximized by decreasing the size of the photovoltaic cells and including an appropriate heat sink to aid convective cooling.

# TABLE OF CONTENTS

	Page
List of Figures	i
List of Tables	iv
<b>Chapter 1: Introduction</b>	<b>1</b>
1.1 Background	2
1.2 Scope	5
1.3 References	6
<b>Chapter 2: LCPV Technology</b>	<b>7</b>
2.1 Optical Sub-System	8
2.2 Electrical Sub-System	10
2.3 Thermal Sub-System	11
2.4 CPV Arrays	12
2.4.1 Rockingham, Australia	12
2.4.2 California, USA	12
2.4.3 Sicily, Italy	12
2.4.4 Qinghai, China	12
2.5 Summary	14
2.6 References	15
<b>Chapter 3: Optical Sub-System</b>	<b>16</b>
3.1 Optical Model	17
3.2 Construction	22
3.3 Summary	23
3.4 References	24

<b>Chapter 4: Electrical Sub-System</b>	25
4.1 Photovoltaic Principles	26
4.1.1 P-N Junction	26
4.1.2 Ideal Solar Cell	27
4.1.2.1 Short Circuit Current	28
4.1.2.2 Open Circuit Voltage	29
4.1.2.3 Maximum Power Point	29
4.1.2.4 Fill Factor	29
4.1.3 Real Solar Cell	30
4.1.3.1 Shunt Resistance	31
4.1.3.2 Series Resistance	32
4.1.4 Concentration Effects	35
4.1.4.1 Short Circuit Current	35
4.1.4.2 Open Circuit Voltage	36
4.1.4.3 Series Resistance	36
4.1.5 Connecting PV cells	38
4.2 1-Sun I-V Characteristics	40
4.2.1 Experimental	40
4.2.2 Results	40
4.3 4.83-Sun I-V Characteristics	43
4.3.1 Experimental	43
4.3.2 Results	43
4.4 Summary	50
4.5 References	51

<b>Chapter 5: Thermal Sub-System</b>	<b>52</b>
5.1 Temperature Effects	53
5.1.1 Intrinsic Carrier Concentration	53
5.1.2 Open Circuit Voltage	55
5.2 Thermal Model	56
5.2.1 Development	56
5.2.2 Validation	58
5.2.2.1 Convective Transfer Co-efficient	58
5.2.2.2 Experimental	60
5.2.2.3 Results	62
5.3 Environmental Conditions	64
5.3.1 Irradiance	64
5.3.1.1 Experimental	64
5.3.1.2 Results	65
5.3.2 Wind Velocity	66
5.3.2.1 Experimental	67
5.3.2.2 Results	67
5.3.3 Ambient Temperature	70
5.4 Electrical Power	71
5.4.1 Experimental	71
5.4.2 Results	72
5.5 Heat Sink	74
5.5.1 Design	74
5.5.2 Experimental	76
5.5.3 Results	77
5.6 Thermal Stress Evaluation	78
5.6.1 Experimental	78
5.6.2 Results	78
5.7 Summary	81
5.8 References	82

<b>Chapter 6: Conclusion</b>	83
6.1 Optical Sub-System	84
6.2 Electrical Sub-System	85
6.3 Thermal Sub-System	87
6.4 Recommendations	89
<b>Appendix: Mathematica Code</b>	90

## LIST OF FIGURES

	Page
Figure 1.1 Carbon emissions since 1980	2
Figure 1.2: PV module cost per watt in the United States	4
Figure 2.1: 1-Axis tracker system at Aquila Game Reserve in South Africa	9
Figure 2.2: Multi-Junction PV cell	13
Figure 2.3: Silicon PV cell	13
Figure 3.1: Conceptual illustration of optical sub-system	17
Figure 3.2: Drawing of 7-facet reflector (Scale 1:3)	19
Figure 3.3: Graph showing geometric concentration ration as a function of number of facets	21
Figure 3.4: Constructed 7-facet reflector system	22
Figure 4.1: Operation of a p-n junction	26
Figure 4.2: I-V characteristic	28
Figure 4.3: 1-diode model with shunt and series resistors	31
Figure 4.4: I-V characteristic showing the effect of shunt resistance	32
Figure 4.5: I-V characteristic showing the effect of series resistance	33
Figure 4.6: I-V characteristics or 1- and 2-cell configuration with series resistance $0.3\Omega$	34
Figure 4.7: I-V characteristics or 1- and 2-cell configuration with series resistance $0.05\Omega$	35
Figure 4.8: I-V characteristic showing the effect of series resistance under concentration	37
Figure 4.9: Concentrated I-V characteristics of 1- and 2-cell configuration with series resistance $0.05\Omega$	38
Figure 4.10: 6-Cell PV receiver	39
Figure 4.11: I-V characteristics of the 8-, 6- and 4-cell under 1-sun conditions at direct irradiance of $1000\text{W}/\text{m}^2$	41
Figure 4.12: I-V characteristics of the 8-, 6- and 4-cell under 4.83-sun conditions at direct irradiance of $1000\text{W}/\text{m}^2$	44
Figure 4.13: Maximum power point and fill factor for the 4-, 6- and 8-cell	46

receivers under concentration

Figure 4.14: I-V characteristic of 4-cell PV receiver under 1-sun and 4.83-sun conditions	47
Figure 4.15: I-V characteristic of 6-cell PV receiver under 1-sun and 4.83-sun conditions	47
Figure 4.16: I-V characteristic of 8-cell PV receiver under 1-sun and 4.83-sun conditions	48
Figure 5.1: Simulated I-V characteristics showing the effect of temperature	54
Figure 5.2: Energy absorption and dissipation in a LCPV system	56
Figure 5.3: Thermal model validation experimental setup	60
Figure 5.4: Graph showing irradiance and various LCPV system temperatures	62
Figure 5.5: Graph showing dependence of PV receiver temperature on irradiance	66
Figure 5.6: Graph showing the dependence of PV receiver temperature on air velocity	68
Figure 5.7: $\log(v)$ vs. $\log(h)$ graph corresponding to data in Table 5.2	69
Figure 5.8: Graph showing PV receiver temperature when 1 W electrical power is extracted	72
Figure 5.9: Graph showing modelled PV receiver temperature when 6.5 W electrical power is extracted	73
Figure 5.10: Simplified illustration of heat sink	74
Figure 5.11: Graph showing temperature difference with/without heat sink	77
Figure 5.12: Graph showing the frequency of PV receiver operating temperatures	79
Figure 5.13: IV characteristics of the PV receiver under concentration conditions before/after thermal stress	80
Figure 6.1: Graph showing geometric concentration ratio as a function of number of facets	84
Figure 6.2: I-V characteristic showing the effect of series resistance under concentration	85
Figure 6.3: I-V characteristics of the 8-, 6- and 4-cell under 4.83-sun	86

conditions at direct irradiance of  $1000\text{W/m}^2$

Figure 6.4: Graph showing the dependence of PV receiver temperature on air velocity 87

Figure 6.5: IV characteristics of the PV receiver under concentration 88  
conditions before/after thermal stress

## LIST OF TABLES

	Page
Table 3.1: Reflector facet length and angle of orientation	18
Table 4.1: I-V parameters of the 8-, 6- and 4-cell receivers	41
Table 4.2: I-V parameters of the 8-, 6- and 4-cell receivers	44
Table 4.3: I-V parameters and effective concentration ratio of the 4-, 6- and 8-cell receivers	49
Table 5.1: Thermal model validation analysis	63
Table 5.2: Convective transfer co-efficient calculation	68
Table 5.3: Various electrical parameters before/after thermal stress	80
Table 6.1: I-V parameters of the 4-, 6- and 8-cell receivers	86

# Chapter 1

## INTRODUCTION

The combustion of fossil fuels has remained the primary source of electricity despite the development of several alternatives. However, devastating environmental effects and rapidly diminishing fossil fuel reserves suggests that it is more important than ever to develop a large-scale, environmentally friendly, renewable source of energy. This chapter briefly discusses the background and scope of this study.

## 1.1 Background

The world's first power station, the Edison Electric Light Station, began operation in London during January 1882. Today, 130 years later, the combustion of fossil fuels accounts for approximately 90% of all greenhouse gas emissions and significantly contributes to the emission of other pollutants, such as sulphur dioxide and heavy metals [1]. These pollutants are harmful to the environment and may ultimately result in climate change. Figure 1.1 shows the steady increase in global carbon emissions since 1980 [2]. Furthermore, it is estimated that the global coal, oil and natural gas reserves will be depleted within 150 years and cost of energy production is expected to increase sharply as these reserves diminish.

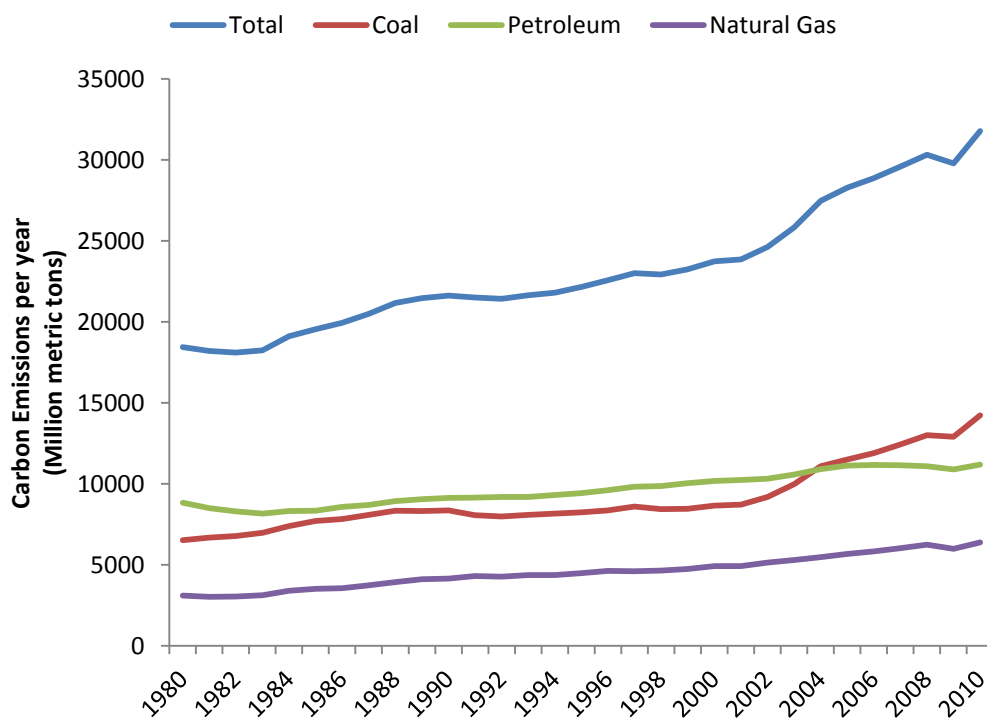


Figure 1.1: Carbon emissions since 1980 [2].

Unfortunately, combustion of fossil fuels continues to be the primary source of energy in the 21<sup>st</sup> century despite the associated environmental hazards. According to the US Energy Information Administration, renewable energy sources account for only 20% of the world's energy production, while coal, oil and gas account for 67%. Nuclear power accounts for the majority of the remaining 13%. Environmentally friendly, renewable sources of energy need to be extensively implemented to ensure long term energy availability and preservation of the environment.

Biomass energy, which involves the burning of plant material, accounts for more than 50% of all energy produced from renewable sources, but the associated pollution still needs to be regulated [2]. Hydro-electric energy also significantly contributes to renewable energy production, but the mechanical nature of the technology increases maintenance costs. Alternatively, photovoltaic (PV) cells are an environmentally friendly, relatively maintenance free source of renewable energy.

Unfortunately, low efficiencies and high production costs have limited the large-scale implementation of PV technology. However, concentrator PV (CPV) technology has the potential to significantly strengthen the PV industry through increased electrical output which translates to lower costs per kWh. A 220 MWh/year HCPV system was recently installed in China, supplying power to approximately 200 000 nearby residents [3]. Unfortunately, HCPV systems are still relatively expensive to manufacture and construct. Alternatively, the cost of silicon solar cells continue to decrease [4], as shown in Figure 1.2, and thus low concentrator photovoltaic (LCPV) systems that use these PV cells may become economically viable in the future. However, further research is necessary to fully understand the optical, electrical and thermal properties of these systems.

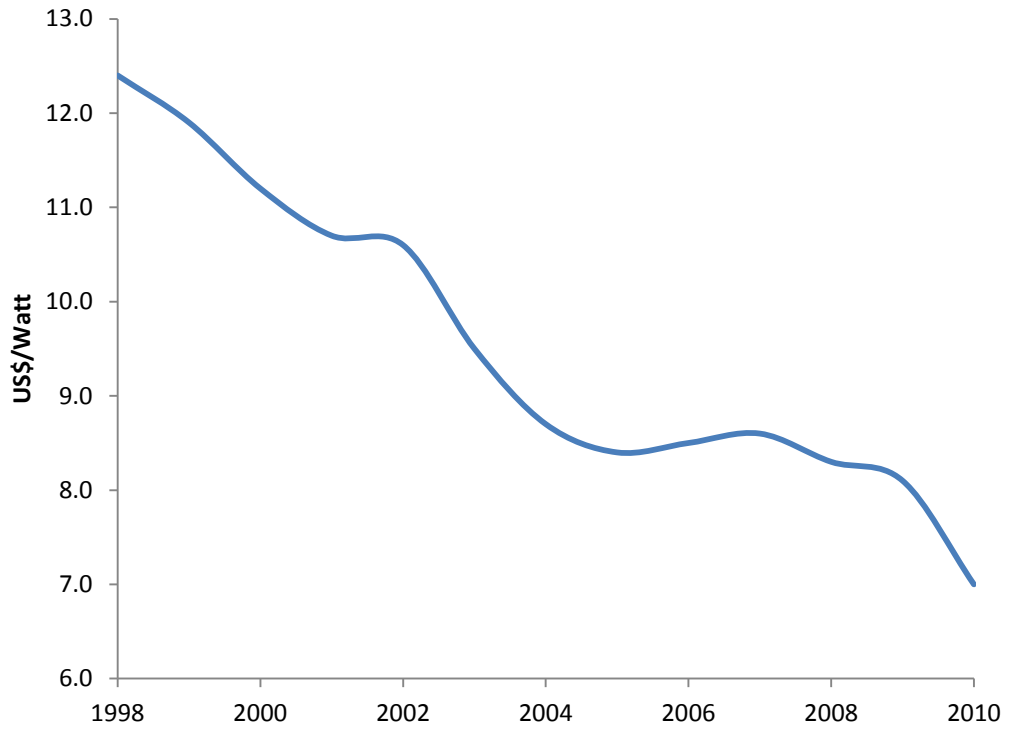


Figure 1.2: PV module cost per watt in the United States.

## 1.2 Scope

The relatively high series resistance associated with silicon PV cells generally leads to increased power losses under concentration conditions. However, the use of small, low current PV cells may significantly reduce these power losses. In this study, several different electrical configurations are investigated theoretically and experimentally to assess the viability of using low current PV cells in LCPV systems. The effect of concentration on various PV parameters, such as short circuit current and fill factor, is also evaluated.

High operating temperatures also cause power losses in LCPV systems. A thermal management system needs to be implemented to ensure the power output of a LCPV system is maximized. In this study, a thermal model is developed to estimate the operating temperatures associated with a LCPV system under various conditions. This model is compared to experimental temperature measurements and is also used to assess the efficiency of a proposed thermal management system. A thermal stress test is performed to evaluate high temperature degradation of the PV cells.

The following chapters discuss the optical-, electrical- and thermal sub-systems of a LCPV system. The results are used to make recommendations towards the design of future LCPV systems.

### 1.3 References

- [1] Caring Planet: The Environmental Website. 2007. Internet: [http://www.caring-planet.com/Page/title/About\\_CO2\\_Emissions/](http://www.caring-planet.com/Page/title/About_CO2_Emissions/) (Accessed: 21 June 2012)
- [2] US Energy Information Administration. 2012. Internet: <http://www.eia.gov/> (Accessed: 3 May 2012)
- [3] PV Magazine. 2012. Internet: [http://www.pv-magazine.com/news/details/beitrag/isofoton-completes-its-first-hcpv-plant-in-china\\_100005235](http://www.pv-magazine.com/news/details/beitrag/isofoton-completes-its-first-hcpv-plant-in-china_100005235) (Accessed: 3 May 2012)
- [4] Barbose, GL, Darghouth, N, Wiser, RH, Seel, J; *Tracking the Sun IV: A Historical Summary of the Installed Cost of Photovoltaics in the United States from 1998 to 2010*; Lawrence Berkeley National Laboratory. Environmental Energy Technologies Division, 2011.

## **Chapter 2**

# **LCPV TECHNOLOGY**

LCPV systems use optical materials to refract or reflect irradiance onto PV cells allowing large areas of PV material to be replaced by lenses or mirrors. Generally, the design of a LCPV system may be divided into 3 sub-systems, namely optical, electrical and thermal. This chapter introduces the optical-, electrical- and thermal sub-systems of a LCPV system and addresses the specific research goals associated with each sub-system. A few examples of CPV arrays are also discussed.

## 2.1 Optical Sub-System

The optical sub-system is an important component of any CPV system as it directly determines the geometric concentration ratio. The geometric concentration ratio ( $X_G$ ) of a CPV system is the ratio of the aperture area of the lenses or mirrors to the area of the PV material. CPV systems are often classified according to the geometric concentration ratio:

High concentrator photovoltaic (HCPV) systems:  $X_G \geq 100$

Low concentrator photovoltaic (LCPV) systems:  $X_G \leq 10$

CPV systems with intermediate geometric concentration ratios ( $10 \leq X_G \leq 100$ ) may be classified as medium concentrator photovoltaic systems [1]. Unfortunately, the effective concentration ratio ( $X_E$ ) is usually less than the geometric concentration ratio due to optical losses associated with refraction and reflection.

The lenses and mirrors used in CPV systems may be used to concentrate irradiance to a point or along a line. Generally, lenses are used to achieve a high geometric concentration ratio by focussing irradiance to a point, whereas mirrors are used to achieve a low geometric concentration ratio by focussing irradiance along a line [2]. However, HCPV and LCPV systems are not restricted to lenses and mirrors, respectively, and may even include a combination of optical materials to meet specific design requirements.

The optical sub-system of a CPV system usually requires that the sun be tracked along 1- or 2-axis to ensure correct optical alignment. For this reason, a mechanical tracker system is essential for effective operation of CPV systems [2, 3]. Figure 2.1 shows a 2-axis tracker used at the Aquila Game Reserve in South Africa.

Experimentally, it is important to evaluate the optical sub-system with respect to effective concentration ratio. This study aims to design and construct an optical sub-system with an effective concentration ratio that is within 10% of the geometric concentration ratio.



Figure 2.1: HCPV system mounted on a 2-axis tracker system at Aquila Game Reserve in South Africa [4]

## 2.2 Electrical Sub-System

The most important part of the electrical sub-system is the PV cells. High efficiency PV cells will transform a greater percentage of incident irradiance into electrical work and consequently maximize electrical power output of the CPV system.

Multi-junction PV cells have efficiencies of up to 43.5% [5] and are capable of operating under high concentration conditions [6]. The high efficiency associated with multi-junction PV cells is the result of a combination of reduced thermalization and transmission losses through the cell and low resistive losses. However, multi-junction cells are relatively expensive to manufacture and are thus reserved for use in HCPV systems [7].

Conventional silicon PV cells have an efficiency of up to 20% [8] and are relatively inexpensive to manufacture. Owing to resistive losses, conventional silicon PV cells are not capable of efficient operation under high concentration conditions, but have the potential to be economically feasible in LCPV systems. Specialist LCPV silicon cells are currently manufactured in small quantities and have an efficiency of approximately 24% under concentration [7].

This study aims to maximize the power output of the electrical sub-system by developing strategies to reduce the resistive losses associated with conventional silicon cells under concentration.

## 2.3 Thermal Sub-System

LCPV systems typically operate at higher temperatures than standard PV systems due to increased incident irradiance per cell area. High operating temperatures reduce the power output of PV cells making it necessary to include a cooling mechanism in the thermal sub-system.

Increasing the amount of energy dissipated by convection is the simplest means of cooling a PV cell. This is accomplished by extending the convective surface area through the addition of a heat sink. Natural convection of air in the vicinity of the heat sink may be sufficient to maintain acceptable operating temperatures under certain conditions. However, the inclusion of a fan to induce forced convection of air may be necessary at higher temperatures. Liquid cooling systems, which pump water through a collection pipes, may be a reasonable consideration in extreme cases. The energy consumption and efficiency of fans and pumps need to be carefully evaluated before implementation [7].

Before a cooling system may be proposed, it necessary to have a thorough understanding of energy transfer and dissipation within a LCPV system. The effect of various environmental conditions, such as air flow velocity and irradiance, on the temperature of the PV cells within the LCPV system need to be evaluated experimentally. Using this information, it should be possible to predict the operating temperature of the PV cells according to the environmental conditions of a specific place or at a specific time. These issues will be addressed experimentally in this study and the results will be used to aid the design of a thermal management system for the LCPV system under investigation.

## **2.4 CPV Arrays**

Several large-scale CPV systems have been installed throughout the world to supply electricity to nearby industrial and residential areas. In some cases, these CPV arrays are also connected to the national electrical grid.

### **2.4.1 Rockingham, Australia**

The Rockingham CPV system was developed by the Australian National University and was connected to the public grid in July 2000. The CPV array, consisting of 152m<sup>2</sup> of silicon PV cells, provides approximately 20 kW. It uses 80 mirrors and a 2-axis tracing system as shown in Figure 2.2 [9].

### **2.4.2 California, USA**

A CPV array, shown in Figure 2.3, was installed on Nichols Farms in California in April 2011. The 1.2 MW CPV array, developed by Bechtel and SolFocus, uses a 650X concentration reflective system to produce 70% of electrical power demand [10].

### **2.4.3 Sicily, Italy**

The installation of the largest grid connected CPV array was completed during June 2012 in Italy. It uses multi-junction PV cells, 2-axis trackers and Fresnel lenses to produce a 1.2 MW peak. Once fully operational, the CPV array will reduce the production of carbon dioxide by approximately 125 tons per year [11].

### **2.4.4 Qinghai, China**

A 100 kW HCPV array was installed in China during 2012. According to Isofoton, the array is capable of producing 50% more energy than conventional PV systems and will supply electricity to approximately 200 000 residents in the Qinghai province [12].



Figure 2.2: CPV array in Rockingham, Australia [9]



Figure 2.3: CPV array in California, USA [10]

## **2.5 Summary**

CPV systems use optical materials to refract or reflect irradiance onto PV cells allowing large areas of PV material to be replaced by lenses or mirrors. Apart from the optical sub-system, an efficient electrical- and thermal sub-system is necessary to maximize the power produced by a CPV system. The following chapters investigate the optimization of the optical-, electrical- and thermal sub-systems of a LCPV system, whilst focussing on the minimization of power losses associated with resistance and temperature.

## 2.6 References

- [1] Andreev, VM, Andreev, VM, Grilikhes, VA, Rumiāntsev, VD; *Photovoltaic Conversion of Concentrated Sunlight*; John Wiley, 1997.
- [2] Luque, A, Hegedus, S; *Handbook of Photovoltaic Science and Engineering*; John Wiley & Sons, 2011.
- [3] McEvoy, A, Markvart, T, Castaner, L; *Practical Handbook of Photovoltaics: Fundamentals and Applications*; Academic Press, 2011.
- [4] Engineering News. 2012. Internet: <http://www.engineeringnews.co.za/article/safari-lodges-concentrated-photovoltaic-plant-could-be-precursor-to-50-mw-project-2010-09-02> (Accessed: 12 November 2012)
- [5] Greentech Solar. 2011. Internet: <http://www.greentechmedia.com/articles/read/solar-junction-setting-new-cpv-efficiency-records/> (Accessed: 3 November 2012).
- [6] RR King, DC Law, CM Fetzer, RA Sherif, KM Edmondson, S Kurtz, GS Kinsey, HL Cotal, DD Krut, JH Ermer, NH Karam; *Pathways to 40%-Efficient Concentrator Photovoltaics*; PVSEC, 2005.
- [7] López, AL, Andreev, VM; *Concentrator Photovoltaics*; Springer, 2010.
- [8] Sunpower. 2012. Internet: <http://www.sunpowercorp.com.au/homes/products-services/solar-panels/> (Accessed: 4 November 2012)
- [9] Photovoltaic Concentrators. 2012. Internet: <http://www.pvresources.com/PVSystems/Concentrators.aspx> (Accessed: 5 August 2012).
- [10] Solfocus. 2012. Intetnet: <http://www.solfocus.com/en/news-events/press-releases/2011-04-01.php> (Accessed: 13 September 2012).
- [11] Soitec. 2012. Internet: <http://www.soitec.com/en/news/press-releases/article-1008/> (Accessed: 13 September 2012).
- [12] PV Magazine. 2012. Internet [http://www.pv-magazine.com/news/details/beitrag/isofoton-completes-its-first-hcpv-plant-in-china\\_100005235](http://www.pv-magazine.com/news/details/beitrag/isofoton-completes-its-first-hcpv-plant-in-china_100005235) (Accessed: 3 May 2012).

## **Chapter 3**

# **OPTICAL SUB-SYSTEM**

The optical sub-system is responsible for concentrating irradiance onto the PV cells and therefore directly determines the geometric concentration ratio of the LCPV system. A comprehensive evaluation of the optical properties of the LCPV system is beyond the scope of this study, however, it is necessary to briefly discuss the basic elements of the optical sub-system. This chapter outlines the design, implementation and construction of an optical sub-system and discusses the corresponding geometric- and effective concentration ratios.

### 3.1 Optical Model

The optical sub-system used in this study is a line focused 7-facet reflector system. Alternatively, a point focused reflector system may be used for high concentration applications [1]. Figure 3.1 shows a conceptual illustration of the reflector system. It is important to note that the active area of the PV receiver is orientated away from the incoming irradiance so that without the faceted reflector system the PV cells do not receive any irradiance.

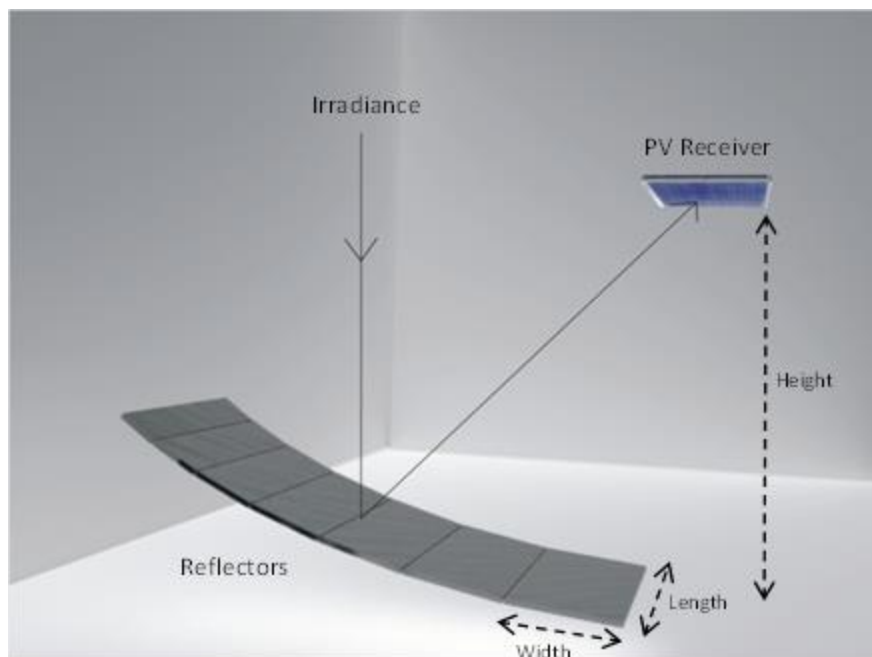


Figure 3.1: Conceptual illustration of optical sub-system

The optical model was designed to meet the following requirements:

- The reflector system must consist of a collection of rectangular facets to facilitate ease of construction.
- Each facet must provide uniform illumination across the PV cells
- The reflector system must provide a satisfactory geometric concentration ( $X_G \approx 5$ ) while restricting the height of LCPV system to a minimum

The length, width and angle of orientation of each reflector facet need to be calculated according to these requirements. As can be seen in Figure 3.1, the length of each reflector facet is simply equal to the length of the PV receiver, but the width of each reflector facet and angle of orientation need to be calculated to meet the design requirements. A program (see appendix) was written in Mathematica to calculate the length of each reflector facet and the corresponding angle of orientation for a given PV receiver height.

The results for a 7-facet reflector system corresponding to a PV receiver height and length of 0.4m and 0.1m respectively are listed in Table 3.1. Figure 3.2 shows a 1:3 scale drawing of a 7-facet reflector system and a PV receiver.

Table 3.1: Reflector facet length and angle of orientation

2Facet	Length (mm)	$\theta$ (°)
1	98	7
2	92	14
3	83	19
4	74	24
5	65	27
6	57	30
7	50	33

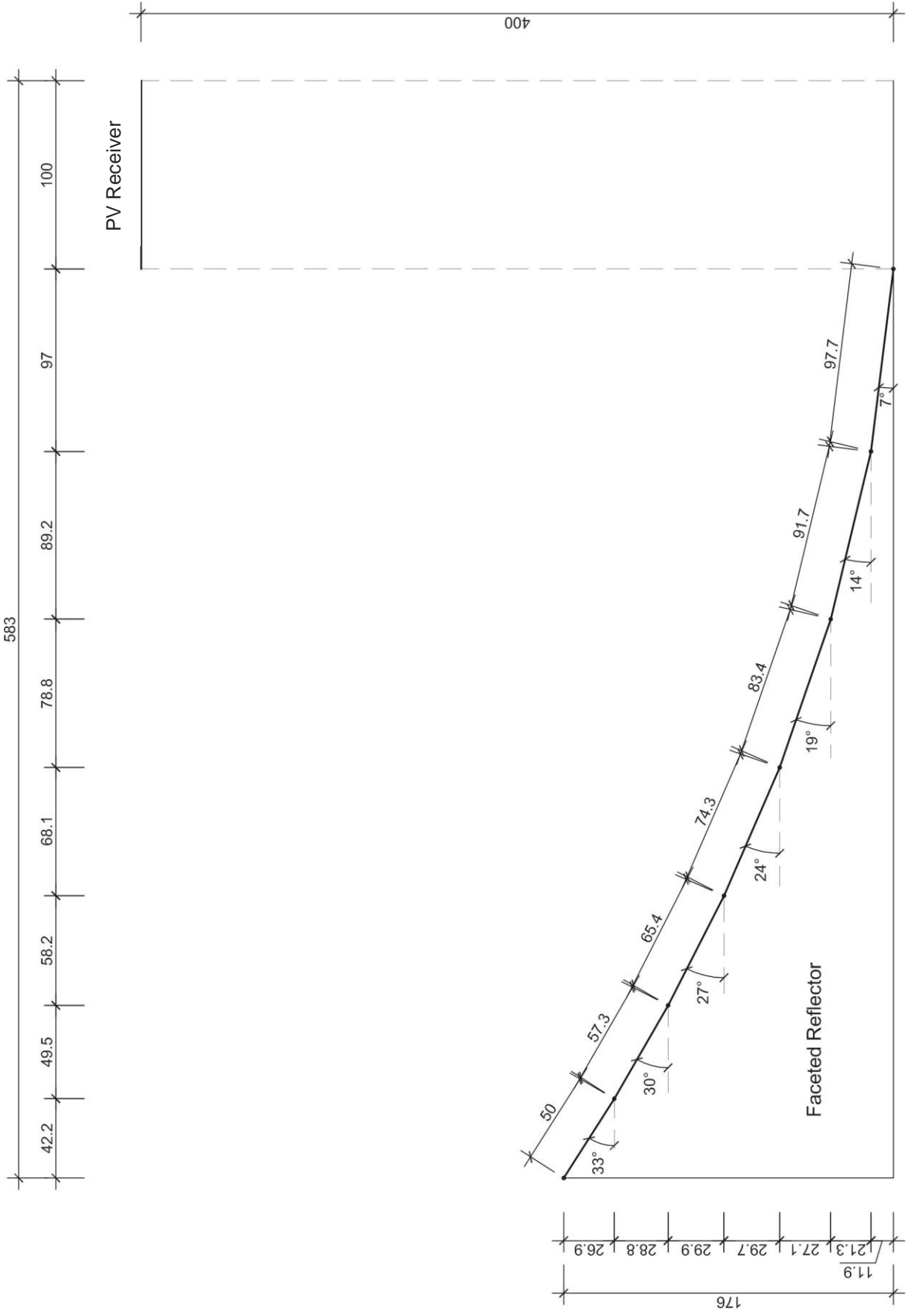


Figure 3.2: Drawing of 7-facet reflector (Scale 1:3)

As mentioned previously, the length of each reflector facet is equal to the length of the PV receiver. For this reason, the geometric concentration ratio, as discussed in Section 2.1, of the optical sub-system is equivalent to the ratio of the total reflector width projected along the horizontal axis to the PV receiver width. The geometric concentration ratio for the optical sub-system used in this study is thus 4.83 as shown in Figure 3.2.

$$X_G = \frac{A_R}{A_M} = \frac{W_R}{W_M} = 4.83 \quad (3.1)$$

$A_R$  is the total projected area of the reflector system and  $A_M$  is the area of the PV receiver.  $W_R$  is the total projected width of the reflector system and  $W_M$  is the width of the PV receiver.

The solar cells within the LCPV system used in this study will thus receive 4.83 times more irradiance, assuming no optical losses, compared to conventional operating conditions without any concentration. However, it is expected that the effective concentration ratio would be slightly less as the optical model does not account for any optical losses. This concentration ratio is a significant improvement on previous LCPV trough designs [2].

The optical model may be used to design a similar optical sub-system consisting of more/less faceted reflectors. Figure 3.3 shows the concentration ratio of the optical sub-system as a function of the number of reflector facets as determined by the optical model.

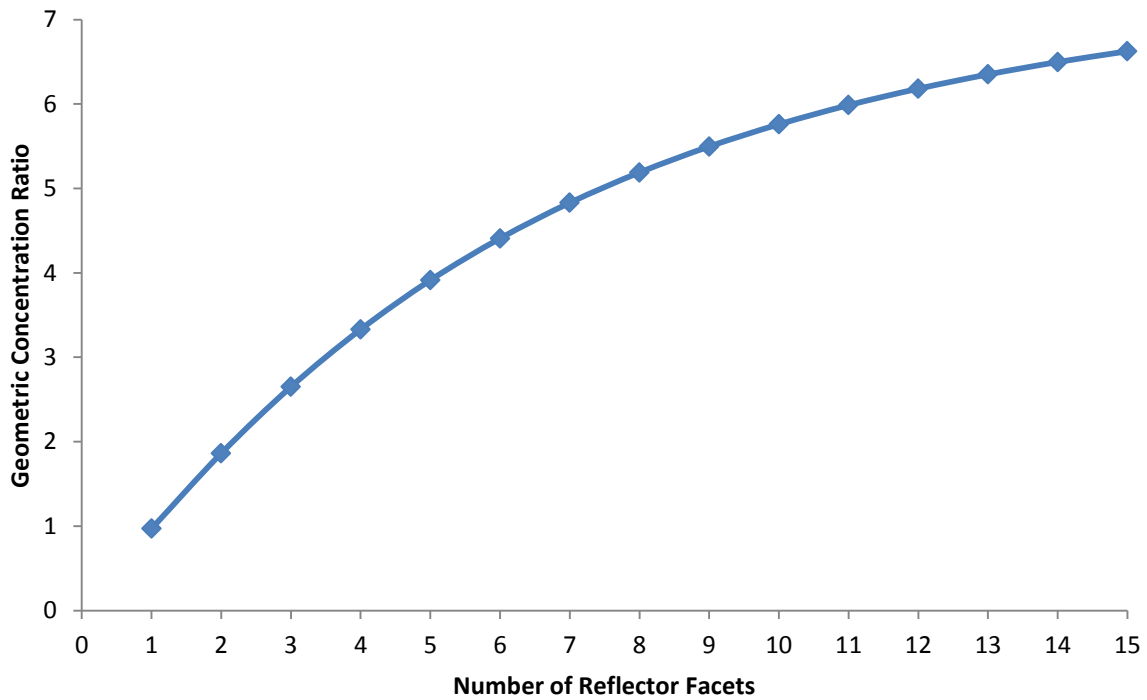


Figure 3.3: Graph showing geometric concentration ratio as a function of number of facets

The geometric concentration ratio contribution of each reflector facet decreases as the number of facets increases. This observation indicates that there exists a finite limit to the geometric concentration ratio associated with the optical model discussed previously. The geometric concentration ratio associated with an optical sub-system consisting of 10 reflector facets is 5.76, but adding an additional 5 reflector facets only increases the geometric concentration ratio by 0.86. It therefore seems reasonable to conclude that constructing an optical sub-system consisting of more than 10-facets would not be financially viable.

### 3.2 Construction

The faceted reflector frame was machined from a 6mm wooden sheet to ensure that the structure was lightweight and rigid. A wooden frame also provides insulation within the LCPV system to facilitate an evaluation of the thermal sub-system as discussed in Chapter 5. Seven reflector facets were cut from a sheet of Alanod PV reflector material [3] and attached to the wooden frame. The Alanod reflector material was evaluated as part of an associated study which indicated that it is more than 95% reflective within the PV spectral range, and thus optical losses are expected to be minimal [4]. An effective concentration ratio of approximately 4.6+ is expected once the reflectivity of the material is taken into account. Figure 3.4 shows the constructed optical sub-system used in this study.



Figure 3.4: Constructed 7-facet reflector system

### **3.3 Summary**

A 7-facet line focussed reflector system was designed and constructed to satisfy the requirements of the optical model as discussed in Section 3.1. The geometric concentration ratio of the optical sub-system used in this study is 4.83, but an effective concentration ratio of 4.6 is expected if an optical loss of 5% is assumed. Upon further analysis of the optical model, it became clear that constructing an optical sub-system consisting of more than 10 reflector facets would not be financially viable. The electrical sub-system is addressed in the following chapter which facilitates the analysis of the performance of the optical sub-system. These results are discussed in Section 4.3.2.

### 3.4 References

- [1] Vivar, M, Anton, I, Sala, G; *Radial CPV receiver*; John Wiley & Sons, 2010.
- [2] BA Butler, *Investigation of Low Concentrator Photovoltaic Modules and Systems*, Masters Thesis, Nelson Mandela Metropolitan University, 2010.
- [3] Alanod Solar. [s.a.]. Internet:  
<http://alanod-solar.com/opencms/opencms/Reflexion/Produkte.html> (Accessed: 4 June 2012)
- [4] MA Benecke, *On the Optical and Electrical Design of LCPV Modules*, Masters Thesis, Nelson Mandela Metropolitan University, 2012.

# Chapter 4

## ELECTRICAL SUB-SYSTEM

The primary goal of any LCPV system is to produce maximum electrical power. This chapter outlines the basic electrical parameters associated with a LCPV system. The chapter focuses on poly-crystalline silicon series connected cells and investigates various configurations aimed at maximizing electrical power. I-V characteristics are measured under conventional (1-Sun) and concentration (4.83-Sun) conditions and the effect of concentration on various electrical parameters is discussed.

## 4.1 Photovoltaic Principles

### 4.1.1 P-N Junction

A silicon solar cell consists of a combination of p-type silicon and n-type silicon to form an electrical junction, called a p-n junction [1]. Figure 4.1 shows a basic illustration of an operational p-n junction. P-type silicon is doped to contain positive holes that do not participate in bonding, whereas n-type silicon is doped to contain negative electrons that do not participate in bonding. At the contact boundary positive holes migrate into the n-type silicon and negative electrons migrate into the p-type silicon. This induces an electric field across the junction and a region that does not contain any mobile charge carriers, called the depletion region, develops.

If a photon of sufficient energy is absorbed by the p-n junction an electron-hole pair will be separated and an electrical current, referred to as a photocurrent, will be produced as a result of the internal electric field. It is important to note that a p-n junction is an electrical diode and the induced voltage will therefore produce a diode current opposite to the produced photocurrent. The current produced by a solar cell is therefore generally less than the photocurrent.

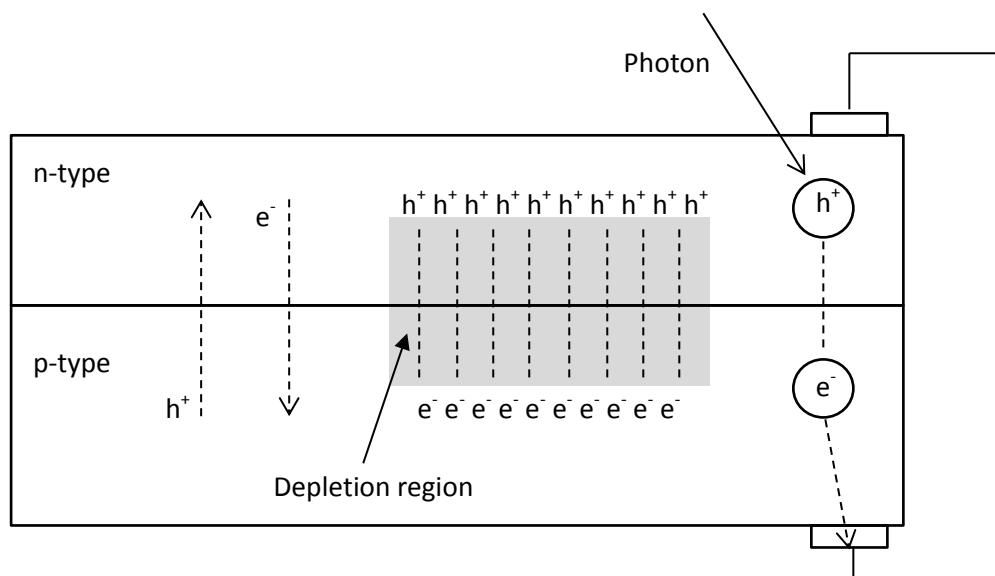


Figure 4.1: Operation of a p-n junction

### 4.1.2 Ideal Solar Cell

The operation of an ideal solar cell can be described in terms of a 2-diode model by the following equation [2]:

$$I = I_L - I_{o1} \left( e^{qV/kT} - 1 \right) - I_{o2} \left( e^{qV/2kT} - 1 \right) \quad (4.1)$$

$I_L$  is the photocurrent generated by photons incident on the p-n junction.  $I_{o1}$  and  $I_{o2}$  are the saturation currents for each diode.  $q$  is the charge of an electron and  $k$  is the Boltzmann constant.  $T$  is the temperature of the solar cell.  $I$  and  $V$  are the current and voltage, respectively.

The second term in equation 4.1 accounts for the diode current due to recombination in the quasi-neutral regions, while the third term in equation accounts for the diode current due to recombination in the depletion region. The third term can be neglected when considering a typical silicon solar cell and equation then reduces to [2]:

$$I \approx I_L - I_{o1} \left( e^{qV/kT} - 1 \right) \quad (4.2)$$

Equation 4.2 is referred to as the 1-diode model. A graph of current vs. voltage is referred to as the I-V characteristic of a solar cell. Figure 4.2 shows a simulated I-V characteristic of an ideal solar cell according to equation 4.2, with  $I_L = 1A$ .

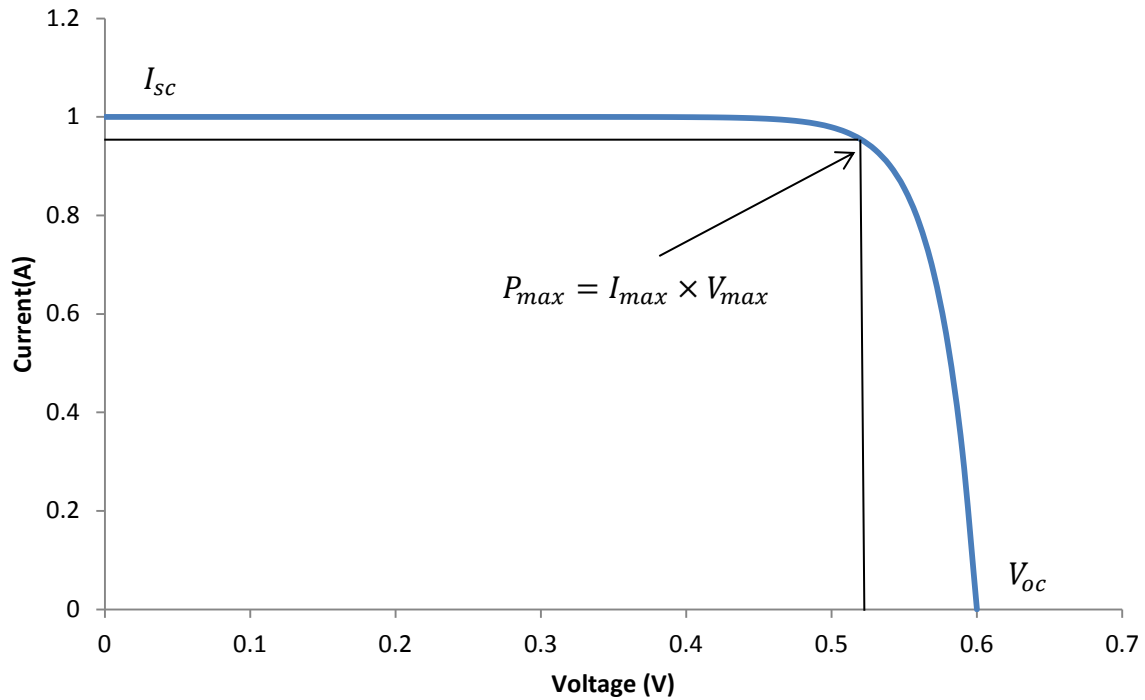


Figure 4.2: I-V characteristic

#### 4.1.2.1 Short Circuit Current

The short circuit current ( $I_{sc}$ ) of a solar cell is defined as the measured current when there is no voltage across the terminals. When the solar cell is in short circuit, the diode current is zero and thus the short circuit current should be equal to the photocurrent. Substituting  $V = 0$  into equation 4.2 yields [1]:

$$I_{sc} \approx I_L \quad (4.3)$$

Since the photocurrent is proportional to irradiance, the short circuit current is also proportional to irradiance.

#### 4.1.2.2 Open Circuit Voltage

The open circuit voltage ( $V_{oc}$ ) of a solar cell is defined as the voltage across the terminals when no current flows. Under these conditions the diode current will be equal and opposite to the photocurrent. Substituting  $I = 0$  into equation 4.2 yields [1]:

$$V_{oc} = \frac{kT}{q} \ln \left( \frac{I_L}{I_{o1}} + 1 \right) = \frac{kT}{q} \ln \left( \frac{I_{sc}}{I_{o1}} + 1 \right) \quad (4.4)$$

Since the photocurrent is directly proportional to irradiance, the open circuit voltage has a logarithmic relationship with irradiance.

#### 4.1.2.3 Maximum Power Point

The maximum power point ( $P_{max}$ ) of a solar cell is defined as the maximum product of current and voltage. The current corresponding to the maximum power point is abbreviated as  $I_{max}$ , while the corresponding voltage is abbreviated as  $V_{max}$ . The maximum power point is determined numerically once the I-V characteristic of a particular solar cell has been measured. The maximum power point is of great significance as it is directly related to the efficiency ( $\eta$ ) of the solar cell [2] by the following equation:

$$\eta = \frac{P_{max}}{\tau A} \quad (4.5)$$

$\tau$  is the irradiance and  $A$  is the aperture area of the PV receiver.

#### 4.1.2.4 Fill Factor

The fill factor ( $FF$ ) of a solar cell is defined as the ratio of maximum power point to the product of short circuit current and open circuit voltage.

$$FF = \frac{P_{max}}{I_{sc} V_{oc}} \quad (4.6)$$

Graphically, fill factor is equivalent to the rectangular area formed under the I-V characteristic by the maximum power point, as shown in Figure 4.2, divided by the rectangular area formed by the short circuit current and open circuit voltage. For a good quality solar cell, the fill factor would approach 1 [3].

#### 4.1.3 Real Solar Cell

The 1- and 2-diode models described in section 4.1.2 do not account for any power losses which may occur as a result of manufacturing imperfections and contact resistances. The 1-diode model of a real solar cell thus includes a shunt ( $R_{sh}$ ) and series ( $R_s$ ) resistor to account for these losses as shown in Figure 4.3. It is important to note that measured voltage ( $V$ ) is not equal to the voltage across junction ( $V_j$ ) due to the voltage drop across the series resistor. The relationship between the measured voltage and junction is given by the following equation:

$$V_j = V + IR_s \quad (4.7)$$

With reference to Equation 4.7, the modified 1-diode model for a real solar cell is described by the following equation [4]:

$$I = I_L - I_{o1} \left( e^{\frac{q(V+IR_s)}{kT}} - 1 \right) - \frac{V + IR_s}{R_{sh}} \quad (4.8)$$

For a given I-V characteristic, all parameters in equation 4.8 can be extracted numerically using appropriate computer software [5].

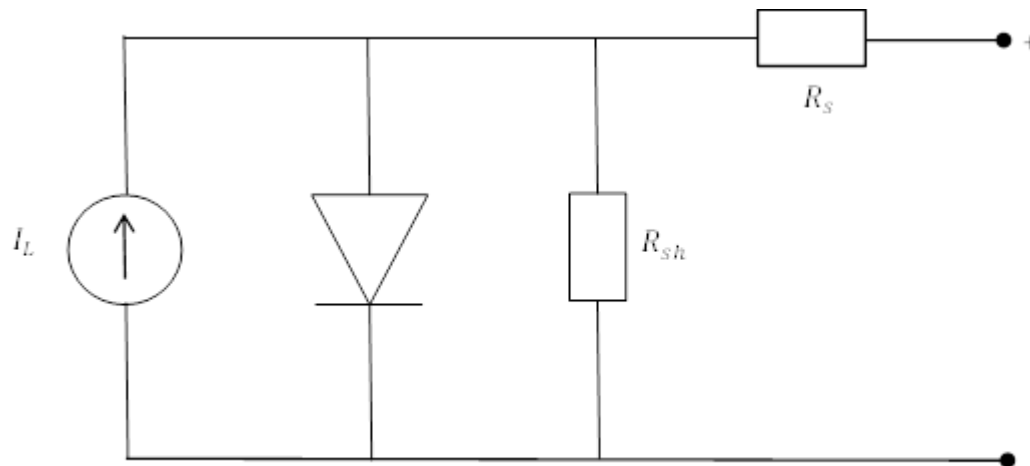


Figure 4.3: 1-diode model with shunt and series resistors.

#### 4.1.3.1 Shunt Resistance

Electrical contact may exist between the front and rear contacts of a solar cell due to manufacturing imperfections, resulting in the development of a shunting path across the p-n junction. A portion of the current may thus bypass the electrical load and flow directly between the front and rear contacts. This reduction in measured current is modelled by the inclusion of a resistor parallel to the photocurrent and diode as shown in Figure 4.3. At a constant measured voltage, a low shunt resistance will increase the contribution of the third term and consequently reduce the measured current according to Equation 4.8. For this reason, the shunt resistance of a solar cell should be as high as possible to maximize power output. A low shunt resistance reduces the fill factor and subsequently the maximum power point decreases [4]. The effect of low shunt resistance is illustrated by the simulated I-V characteristic as shown in Figure 4.4. The fill factor of the I-V characteristic corresponding to a shunt resistance of  $50\Omega$  is 0.82, while the fill factor of the I-V characteristic corresponding to a shunt resistance of  $5\Omega$  is 0.74.

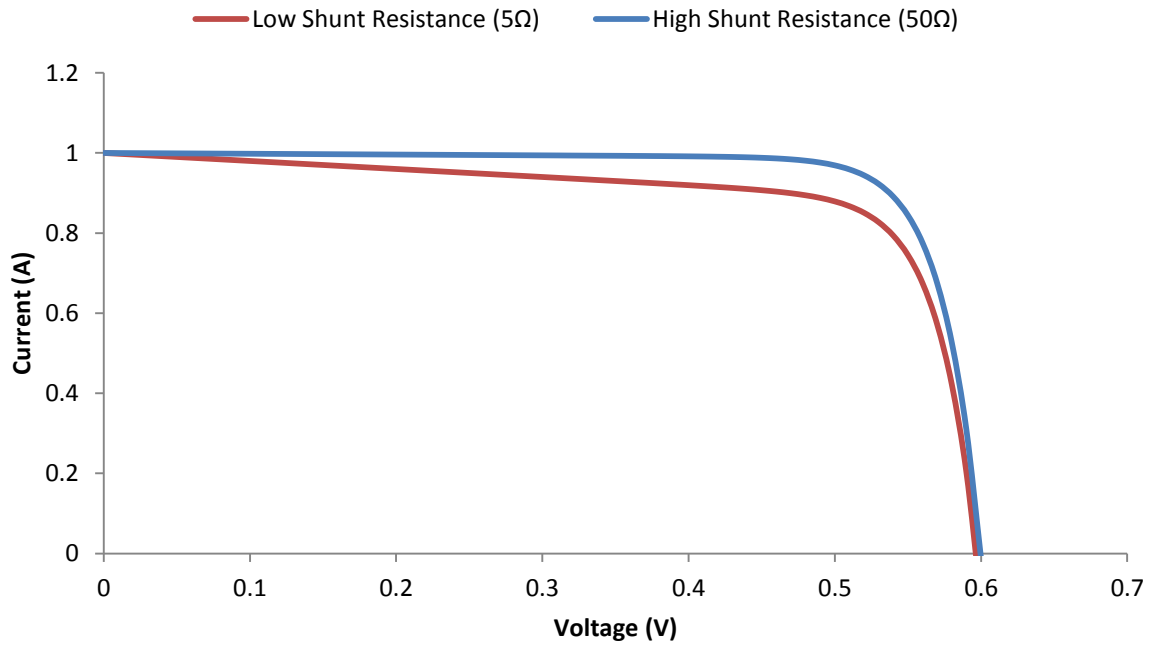


Figure 4.4: I-V characteristic showing the effect of shunt resistance

#### 4.1.3.2 Series Resistance

The contact resistances of a real solar cell have a finite value which needs to be accounted for. The resistance of the electrical contacts is modelled by the inclusion of a resistor in series with the electrical load as shown in Figure 4.3. At a constant measured voltage, a high series resistance will increase the contribution of the second term and consequently limit the measured current according to equation 4.8. For this reason, the series resistance of a solar cell should be as low as possible to maximize power output [4].

The effect of high series resistance is illustrated by the simulated I-V characteristic as shown in Figure 4.5. The fill factor of the I-V characteristic corresponding to a series resistance of  $0.1\Omega$  is 0.68, while the fill factor of the I-V characteristic corresponding to a shunt resistance of  $0.3\Omega$  is 0.42. It is clear that a high series resistance reduces the maximum power point and consequently the fill factor is reduced according to Equation 4.6 [6]. This relationship between fill factor and series resistance is also present for high efficiency multi-junction cells [7].

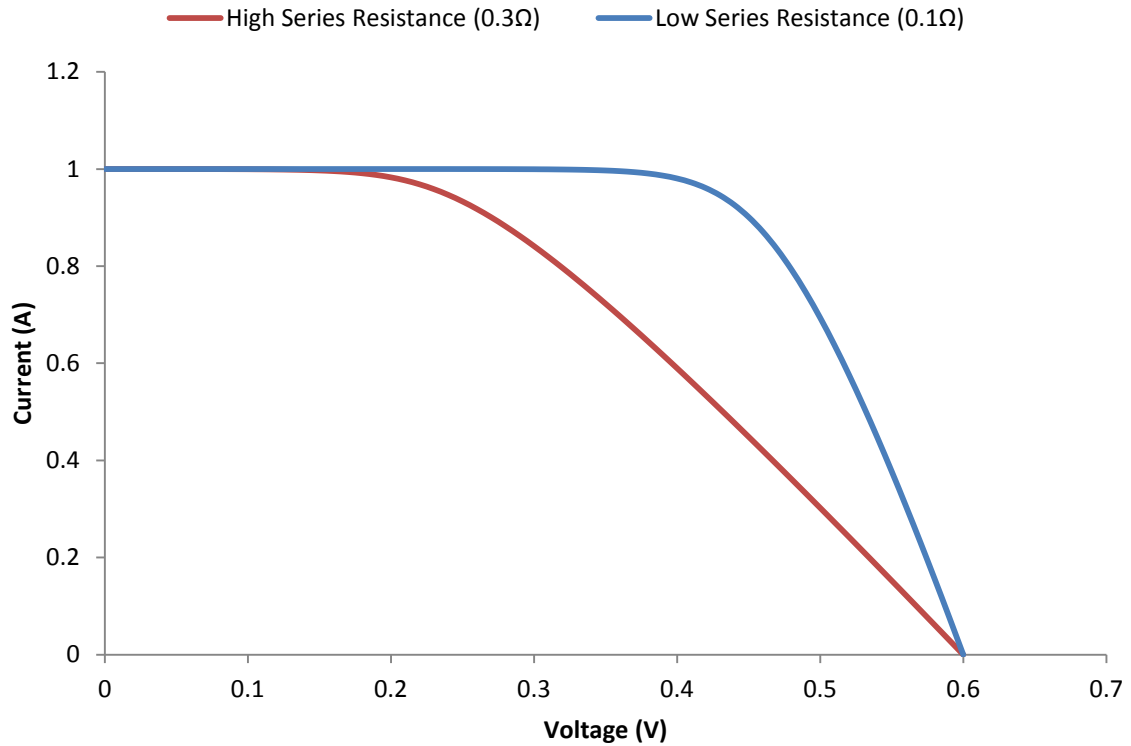


Figure 4.5: I-V characteristic showing the effect of series resistance

The power loss associated with the series resistor may also be described by the following equation:

$$P_{loss} = I^2 R \quad (4.9)$$

Equation 4.9 suggests that it is necessary to lower the current or series resistance of a PV cell to minimize the power loss. Series resistance, which is often introduced during the manufacturing process, is difficult to control, but the PV cell current is easily decreased by reducing the active cell area. The concept of increasing the maximum power point through the use of smaller, low current, PV is experimentally investigated in Section 4.3.

Consider a PV cell, with series resistance  $0.3\Omega$ , corresponding to the simulated I-V characteristic in Figure 4.5. If the PV cell was divided into 2 parts and connected in series, the short circuit current of the 2-cell configuration would be half of the 1-cell configuration. Similarly, the open circuit voltage of the 2-cell configuration would be twice that of the 1-cell configuration. Since the power loss associated with the series resistor is proportional to  $I^2$ , it is expected that the power loss of the 2-cell configuration would be less than the power loss of the 1-cell configuration. Figure 4.6 shows a simulated I-V characteristic of 1- and 2-cell configuration corresponding to a series resistance of  $0.3\Omega$  per cell. The fill factor of the 2-cell configuration is 0.61, while the fill factor of the 1-cell configuration is 0.42. Since the product of short circuit current and open circuit voltage remains unchanged, the maximum power point is proportional to the fill factor according to equation 4.6 and subsequently the maximum power point of the 2-cell configuration is greater than the maximum power point of the 1-cell configuration.

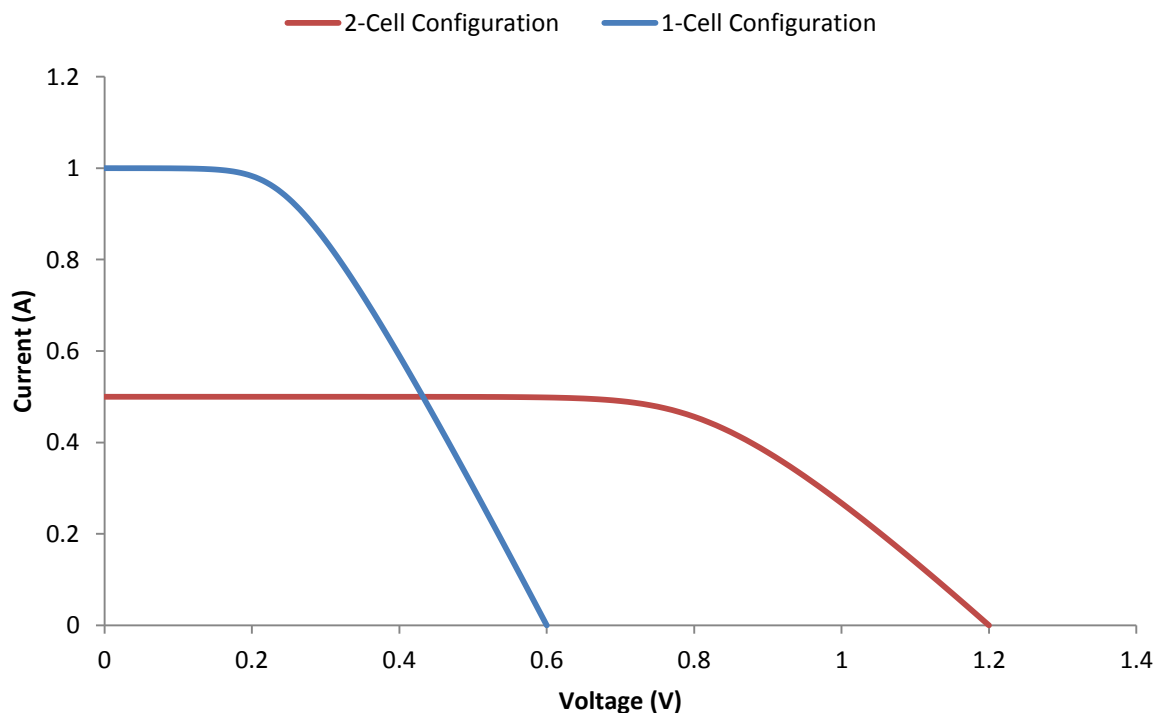


Figure 4.6: I-V characteristics of 1- and 2-cell configuration with series resistance  $0.3\Omega$

It is important to note that if the series resistance is sufficiently low the difference in fill factor may not be as significant. Figure 4.7 shows the simulated I-V characteristics of a 2- and 1-cell configuration corresponding to a series resistance of 0.05 per cell. The fill factor of the 2-cell configuration is 0.79, while the fill factor of the 1-cell configuration is 0.75.

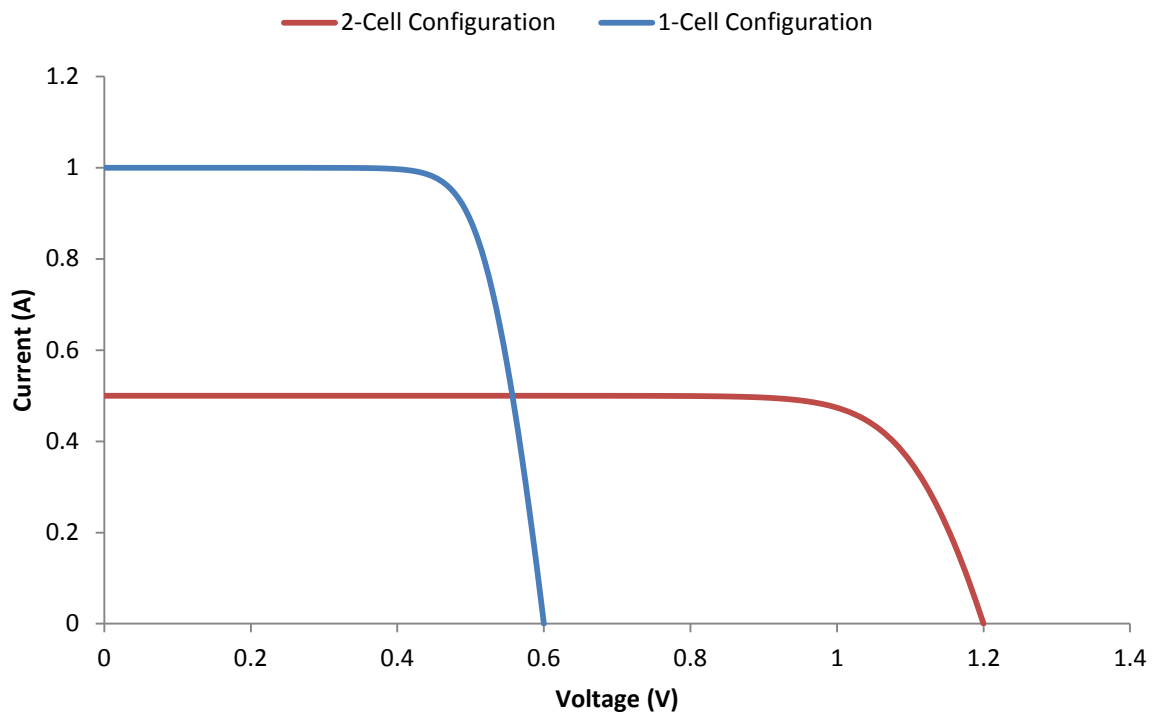


Figure 4.7: I-V characteristics of 1- and 2-cell configuration with series resistance 0.05Ω

#### 4.1.4 Concentration Effects

Concentrated irradiance has numerous effects on the electrical parameters of a solar cell. The short circuit current and open circuit voltage are increased under concentration, but power losses associated with series resistance may become more significant.

##### 4.1.4.1 Short Circuit Current

The short circuit current, which is proportional to irradiance, increases by a factor equal to the concentration ratio ( $X$ ) and is given by the following equation [4]:

$$I_{sc}^X = X I_{sc}^1 \quad (4.10)$$

$I_{sc}^X$  is the short circuit current under concentration.

#### 4.1.4.2 Open Circuit Voltage

The open circuit voltage, which has a logarithmic relationship with irradiance, is given by the following equation [4]:

$$V_{oc}^X = V_{oc}^1 + \frac{kT}{q} \ln(X) \quad (4.11)$$

$V_{oc}^X$  is the open circuit voltage under concentration.

#### 4.1.4.3 Series Resistance

Owing to the high currents associated with a LCPV system, series resistance may be more significant under concentration [8, 9]. The increased current of the PV cell under concentration significantly increases the contribution of the second term in equation 4.7 and subsequently the measured current decreases as discussed in Section 4.1.3.2. This effect is illustrated by a simulated I-V characteristic [10] corresponding to a series resistance of  $0.1\Omega$  as shown in Figure 4.8. The I-V characteristic corresponding to 1X concentration has a fill factor 0.68, while the I-V characteristic corresponding to 3X concentration has a fill factor of 0.44.

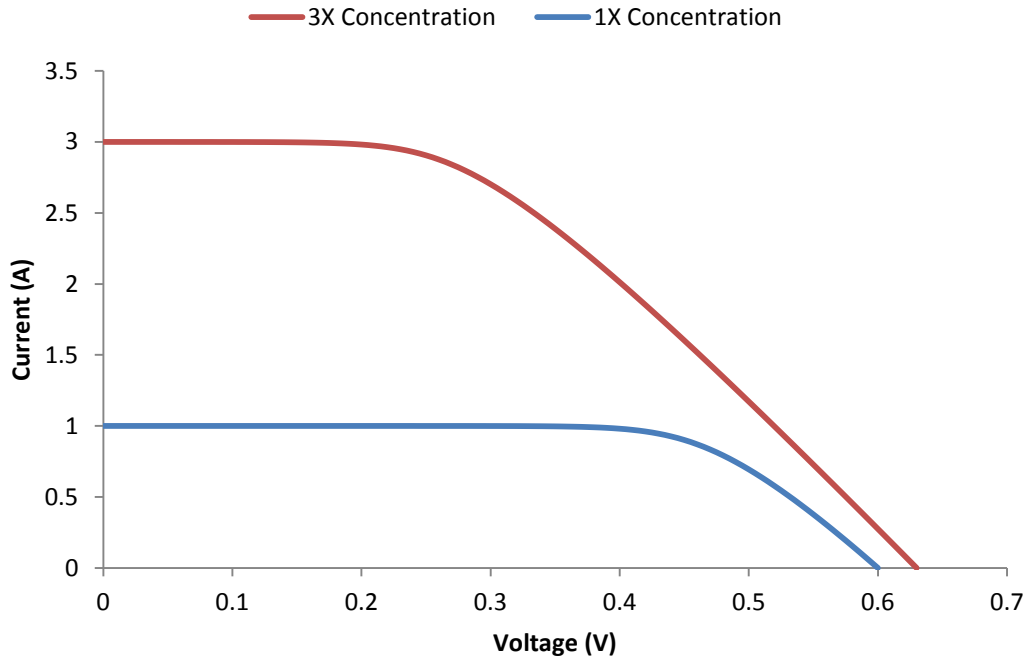


Figure 4.8: I-V characteristic showing the effect of series resistance under concentration

With reference to the I-V characteristics in Figure 4.8, the maximum power point should increase by a factor of 3 if the fill factor was unchanged under concentration according to Equation 4.8. However, the maximum power point only increased by a factor of 1.85 due to the reduced fill factor. As discussed in Section 4.1.3.2, the power loss associated with the series resistor is given by Equation 4.9. However, the power loss under concentration conditions is greater than the power loss under conventional conditions by a factor equal to the square of the concentration ratio as given by the following equation:

$$P_{loss} = X^2 I_1^2 R \quad (4.11)$$

For this reason, the difference in fill factor between the 1- and 2-cell configurations, as discussed in Section 4.1.3.2, is significant even at low series resistance. Figure 4.9 shows the simulated I-V characteristics of a 2- and 1-cell configuration under 3X concentration corresponding to a series resistance of 0.05. The fill factor of the 2-cell configuration is 0.73, while the fill factor of the 1-cell configuration is 0.62. In accordance with Equation 4.9, the maximum power point of the 2-cell configuration is significantly greater than that of the 1-cell configuration. This indicates that it may be necessary to use small, low current PV cells to maximize the power output of a LCPV system.

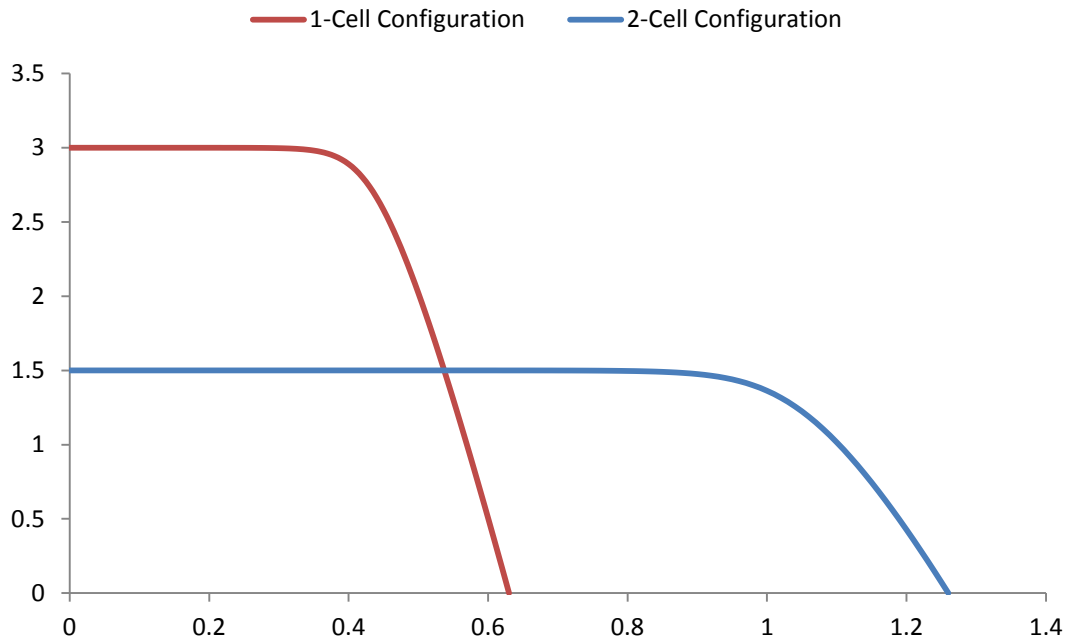


Figure 4.9: Concentrated I-V characteristics of 1- and 2-cell configuration with series resistance  $0.05\Omega$

#### 4.1.5 Connecting PV cells

A collection of PV cells connected in either series or parallel is called a PV cell string. When PV cells are connected in series the open circuit voltage of the PV receiver ( $V_{oc}^M$ ) is equivalent to the product of the number of cells in the PV receiver ( $N$ ) and the open circuit voltage of a single cell ( $V_{oc}^C$ ).

$$V_{oc}^M = NV_{oc}^C \quad (4.10)$$

When PV cells are connected in parallel the short circuit current of the PV receiver ( $I_{sc}^M$ ) is the product of the number of cells in the PV receiver ( $N$ ) and the short circuit current of a single cell ( $I_{sc}^C$ ).

$$I_{sc}^M = NI_{sc}^C \quad (4.11)$$

It may also be desirable to include a combination of series and parallel connections to meet specific electrical requirements.

Three different PV receivers, namely 4-, 6- and 8-cell configurations, of equal total cell area were manufactured for the purpose of this study. The cells were bonded to an aluminium sheet using a phase change material [11] as shown in Figure 4.10.

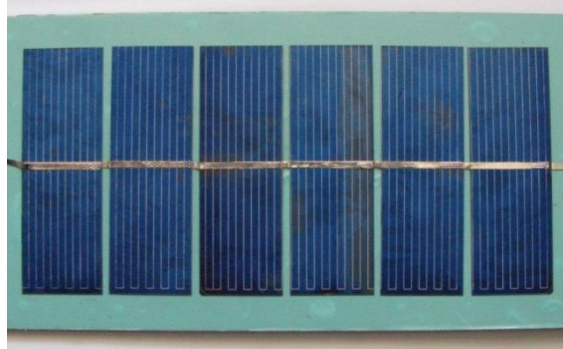


Figure 4.10: 6-Cell PV receiver

## **4.2 1-Sun I-V Characteristics**

The following experiment aims to determine the short circuit current, open circuit voltage, fill factor and the maximum power point for each PV receiver under a geometric concentration ratio of 1 (1-sun conditions).

### **4.2.1 Experimental**

Each PV receiver was mounted on a 2-axis tracker. An I-V tracer was used to measure the I-V characteristics of each PV receiver under 1-sun conditions. All measurements were conducted on clear days in February 2012. Current measurements were normalized to a direct irradiance of 1000 W/m<sup>2</sup>. The PV receiver temperature was 25±3°C for all measurements and for this reason the effect of temperature is considered to be negligible.

### **4.2.2 Results**

Figure 4.10 shows the I-V characteristics of the 4-, 6- and 8-cell PV receiver under standard conditions. The 4-cell PV receiver has the highest short circuit current of 1.13 A, while the 8-cell PV receiver has the highest open circuit voltage of 4.73 V. Table 4.1 lists a comparison of the electrical parameters of each PV receiver. Shunt and series resistances are extracted numerically.

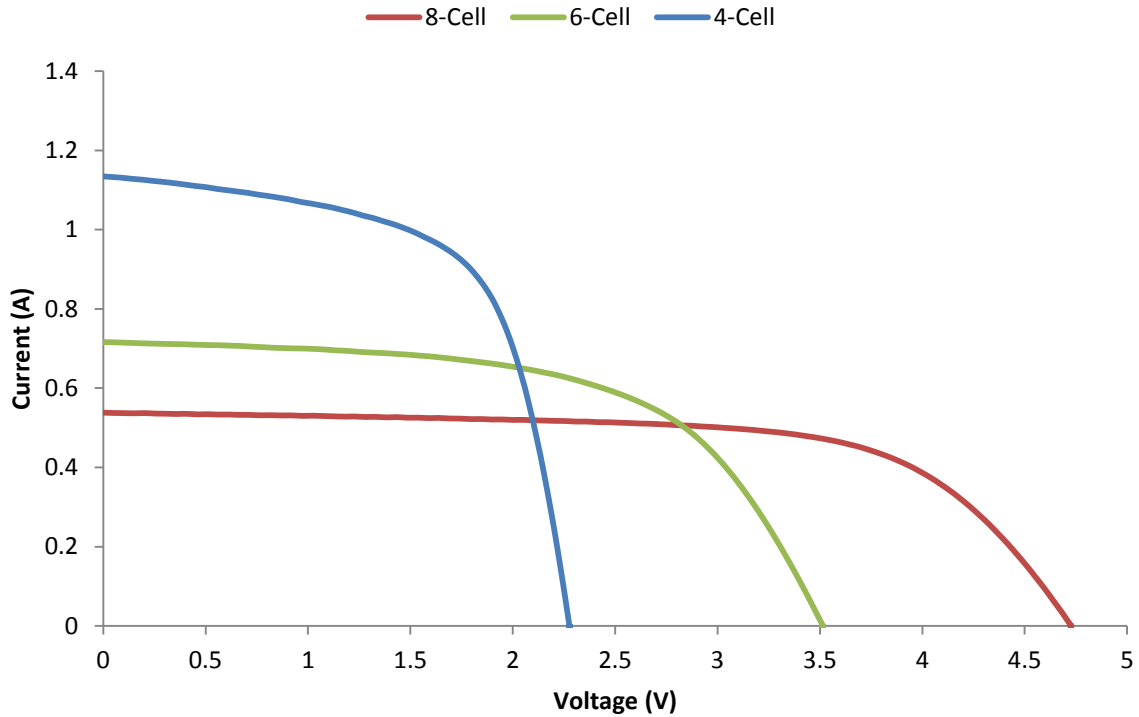


Figure 4.11: I-V characteristics of the 8-, 6- and 4-cell under 1-sun conditions at direct irradiance of 1000W/m<sup>2</sup>

Table 4.1: I-V parameters of the 8-, 6- and 4-cell receivers

	4-Cell	6-Cell	8-Cell
$I_{sc}$	1.13±0.01 A	0.72±0.01 A	0.54±0.01 A
$V_{oc}$	2.28±0.05 V	3.51±0.05 V	4.73±0.05 V
$P_{max}$	1.62±0.05 W	1.48±0.04 W	1.67±0.04 W
$FF$	0.63±0.02	0.59±0.02	0.65±0.02
$R_s$	0.01 Ω	0.07 Ω	0.04 Ω
$R_{sh}$	13 Ω	12 Ω	51 Ω

The 4-cell PV receiver, having the largest cell area per cell, has the highest short circuit current, while the 8-cell PV receiver, having the smallest cell area per cell, has the lowest short circuit current. It should also be noted that the short circuit current of the 4-cell PV receiver is approximately 1.5 times greater than the short circuit current of the 6-cell receiver. This result is expected since the area per cell of the 4-cell PV receiver is 1.5 times greater than that of the 6-cell PV receiver. A similar relationship is also valid when comparing the 6-cell PV receiver to the 8-cell PV receiver.

The 8-cell PV receiver has the highest open circuit voltage, while the 4-cell has the lowest open circuit voltage. The PV receiver with the most individual cells will have the highest open circuit voltage as discussed in Section 4.1.5. It should also be noted that the open circuit voltage of the 8-cell is approximately 1.35 times greater than the open circuit voltage of the 6-cell PV receiver. This result is expected since the 8-cell PV receiver has approximately 1.33 times more individual cells than the 6-cell PV receiver. A similar relationship is also valid when comparing the 6-cell PV receiver to the 4-cell PV receiver.

The 8-cell PV receiver has the highest maximum power point of 1.67 W, while the 6-cell PV receiver has the lowest maximum power point of 1.48 W. The relationship between fill factor and maximum power point, as discussed in Section 4.1.2.4, is clearly illustrated as the 8-cell PV receiver has the highest fill factor and the 6-cell PV receiver has the lowest fill factor. Ideally, it is expected that all the PV receivers would produce similar maximum power as the total cell area of each PV receiver is the same. The 4-cell PV receiver has a similar maximum power point to the 8-cell PV receiver, but the 6-cell PV receiver has a lower maximum power point when compared to the 4- and 8-cell PV receivers. The 6-cell PV receiver has the highest series resistance and the lowest shunt resistance which provides an explanation for the low fill factor and maximum power point in accordance with Sections 4.1.3.1 and 4.1.3.2.

According to these results there is no clear evidence that reducing the individual cell area, and consequently the short circuit current, will result in an increased maximum power point as proposed in Section 4.1.4.3. The effect of series resistance under concentration will be discussed in Section 4.3.

### **4.3 4.83-Sun I-V Characteristics**

This experiment aims to determine the short circuit current, open circuit voltage, fill factor and the maximum power point for each receiver under a geometric concentration ratio of 4.83 (4.83-sun conditions). These parameters are compared to those measured under standard conditions to assess the performance of the LCPV system.

#### **4.3.1 Experimental**

The LCPV system, as described in Chapter 3, was mounted on a 2-axis tracker and each PV-receiver was alternately inserted. An I-V tracer was used to measure the I-V characteristics of each PV receiver under concentrator conditions. All measurements were conducted on clear days in February 2012. Current measurements were corrected to a direct irradiance of  $1000 \text{ W/m}^2$ . Voltage measurements were corrected for temperature to  $25^\circ\text{C}$  using a temperature co-efficient of  $-0.002 \text{ V/}^\circ\text{C}$  per cell [12].

#### **4.3.2 Results**

Figure 4.11 shows the I-V characteristics of the 4-, 6- and 8-cell PV receiver under 4.83-sun conditions. The 4-cell PV receiver has the highest short circuit current of 5.28 A, while the 8-cell PV receiver has the highest open circuit voltage of approximately 4.88 V. Table 4.2 lists a comparison of the electrical parameters of each PV receiver under 4.83-sun conditions.

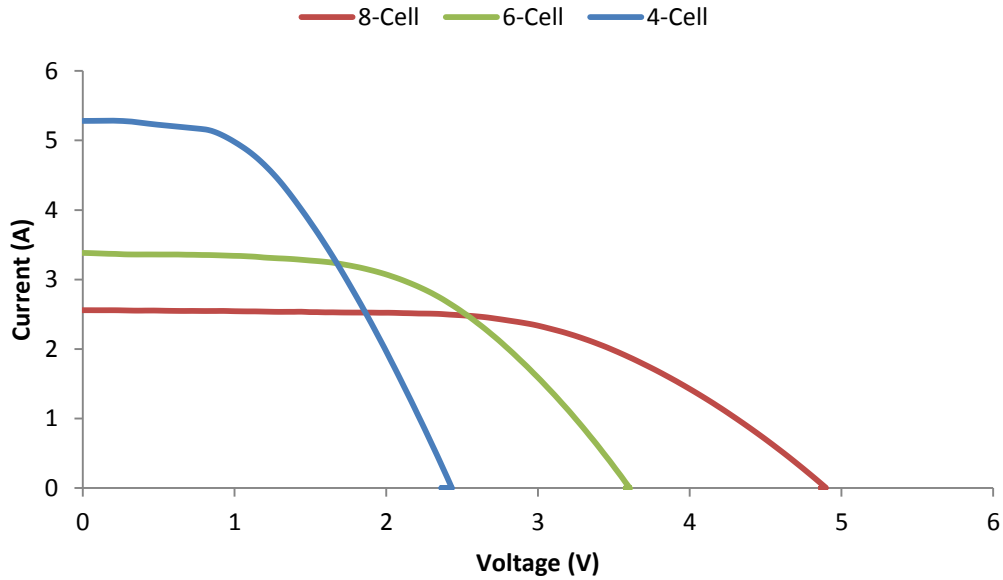


Figure 4.12: I-V characteristics of the 8-, 6- and 4-cell under 4.83-sun conditions at direct irradiance of 1000W/m<sup>2</sup>

Table 4.2: I-V parameters of the 8-, 6- and 4-cell receivers

	4-Cell	6-Cell	8-Cell
$I_{sc}$	5.28±0.01 A	3.38±0.01 A	2.56±0.01 A
$V_{oc}$	2.43±0.05 V	3.61±0.05 V	4.88±0.05 V
$P_{max}$	5.78±0.20 W	6.50±0.14 W	7.13±0.11 W
$FF$	0.45±0.02	0.53±0.01	0.57±0.01
$R_s$	0.04 Ω	0.03 Ω	0.05 Ω
$R_{sh}$	21 Ω	28 Ω	38 Ω

Once again, the 4-cell, having the largest cell area per cell, has the highest short circuit current, while the 8-cell, having the smallest cell area per cell, has the lowest short circuit current. The short circuit current of the 4-cell PV receiver is approximately 1.5 times greater than the short circuit current of the 6-cell PV receiver. A similar relationship is also valid when comparing the 8-cell PV receiver to the 6-cell PV receiver.

The 8-cell PV receiver has the highest open circuit voltage, while the 4-cell has the lowest open circuit voltage. The PV receiver with the most individual cells will generally have the highest open circuit voltage as discussed in Section 4.1.5. The open circuit voltage of the 8-cell is approximately 1.35 times greater than the open circuit voltage of the 6-cell PV receiver. A similar relationship is also valid when comparing the 6-cell PV receiver to the 4-cell PV receiver. These results identical are to those obtained under 1-sun conditions as discussed in Section 4.2.2.

The 8-cell PV receiver has the highest maximum power point of 7.13 W, while the 4-cell PV receiver has the lowest maximum power point of 5.78 W. The 8-cell PV receiver has the highest fill factor and the 4-cell PV receiver has the lowest fill factor. The relationship between maximum power point and fill factor is once again confirmed as discussed in Section 4.1.2.4. It is clear that the best performing PV receiver, in terms of maximum power point and fill factor, is the 8-cell PV receiver ( $I_{sc} = 2.56$ ), while the worst performing PV receiver is the 4-cell PV receiver ( $I_{sc} = 5.28$ ). The 6-cell PV receiver ( $I_{sc} = 3.38$ ) has an intermediate maximum power point and fill factor with respect to the 4- and 8-cell PV receivers. It is important to note that each PV receiver has approximately the same series resistance and thus the reduced maximum power point and fill factor of the 4- and 6-cell PV receivers should not be attributed directly to series resistance. However, the amplification of series resistance at higher currents significantly reduces the maximum power point and fill factor of the 4- and 6-cell PV receivers. Figure 4.13 shows the maximum power point and fill factor of each PV receiver under concentration.

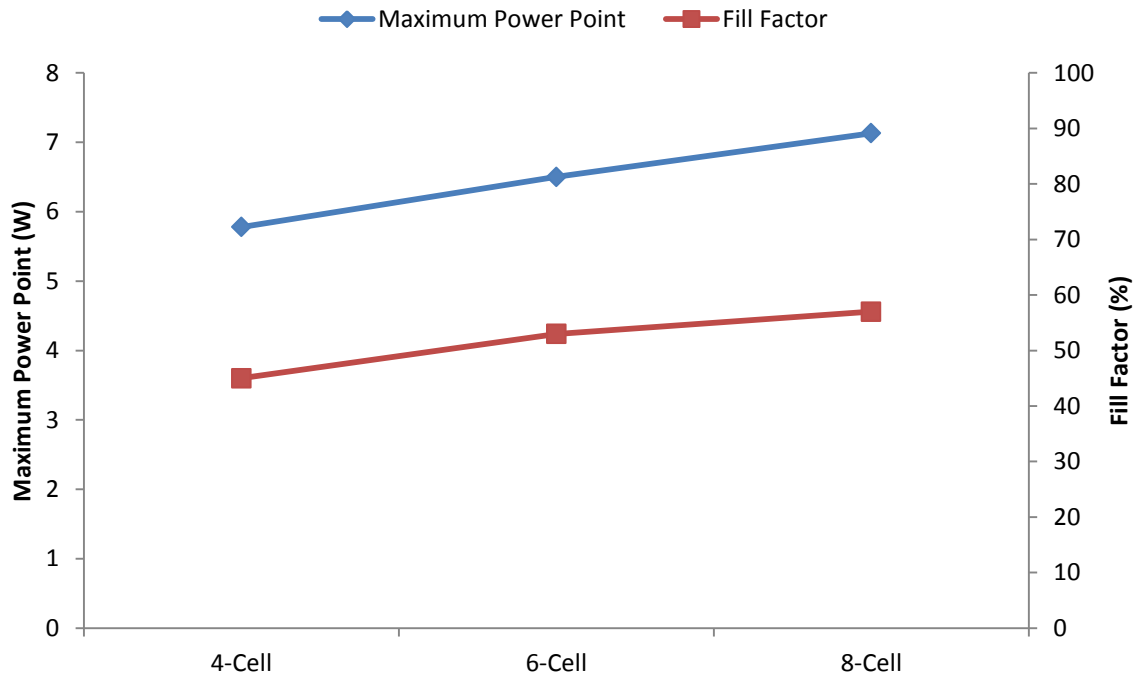


Figure 4.13: Maximum power point and fill factor for the 4-, 6- and 8-cell receivers under concentration

The results indicate that a PV receiver with a high short circuit current will have a lower fill factor than a PV receiver with a low short circuit current. This observation has been discussed and theoretically modelled in Section 4.1.4.3. These results clearly indicate that it is necessary to lower the short circuit current, through the use of smaller PV cells, to maximize the power output under concentration.

In order to assess the performance of the optical sub-system it is necessary to compare the electrical parameters of each PV receiver under standard and concentration conditions. Figures 4.14 – 4.16 show the I-V characteristics under standard and concentration conditions for each PV receiver. Table 4.3 shows a comparison of the electrical parameters under 1-sun and 4.83-sun conditions as well as the effective concentration ratio calculated from Equation 4.10.

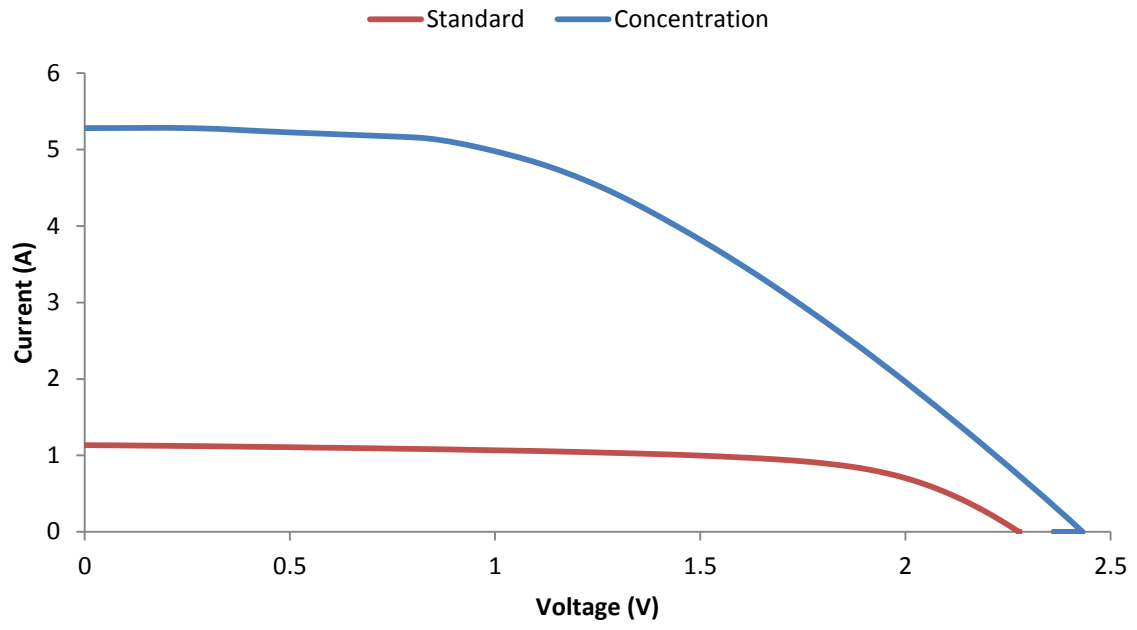


Figure 4.14: I-V characteristic of 4-cell PV receiver under 1-sun and 4.83-sun conditions

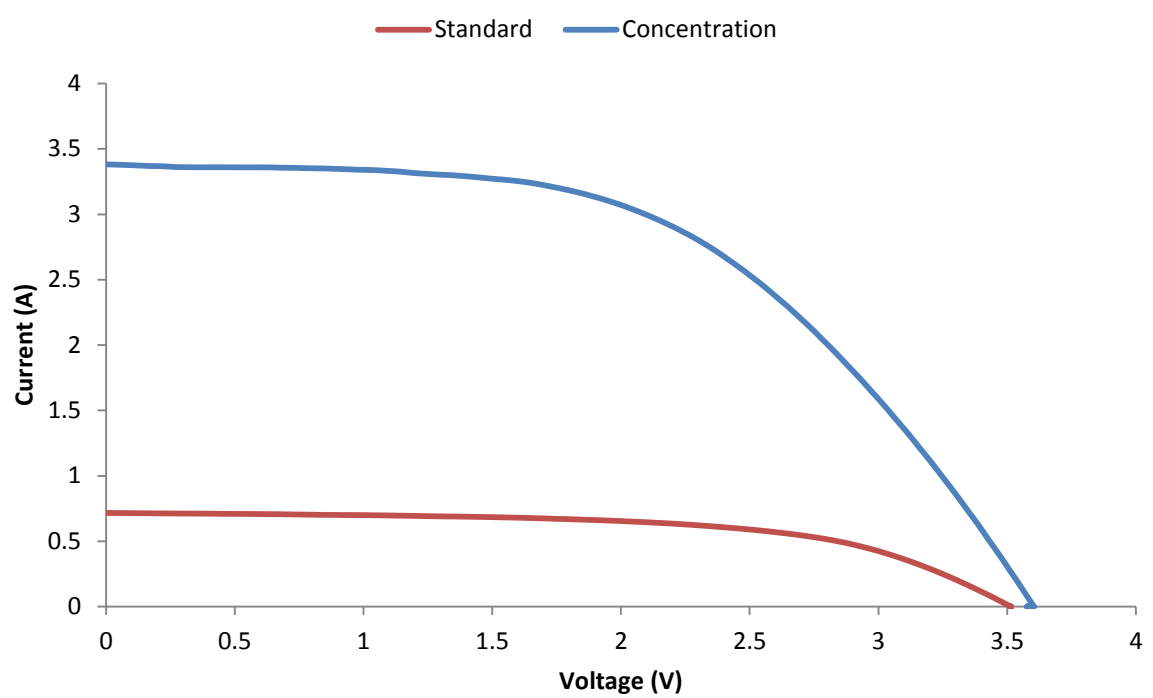


Figure 4.15: I-V characteristic of 6-cell PV receiver under 1-sun and 4.83-sun conditions

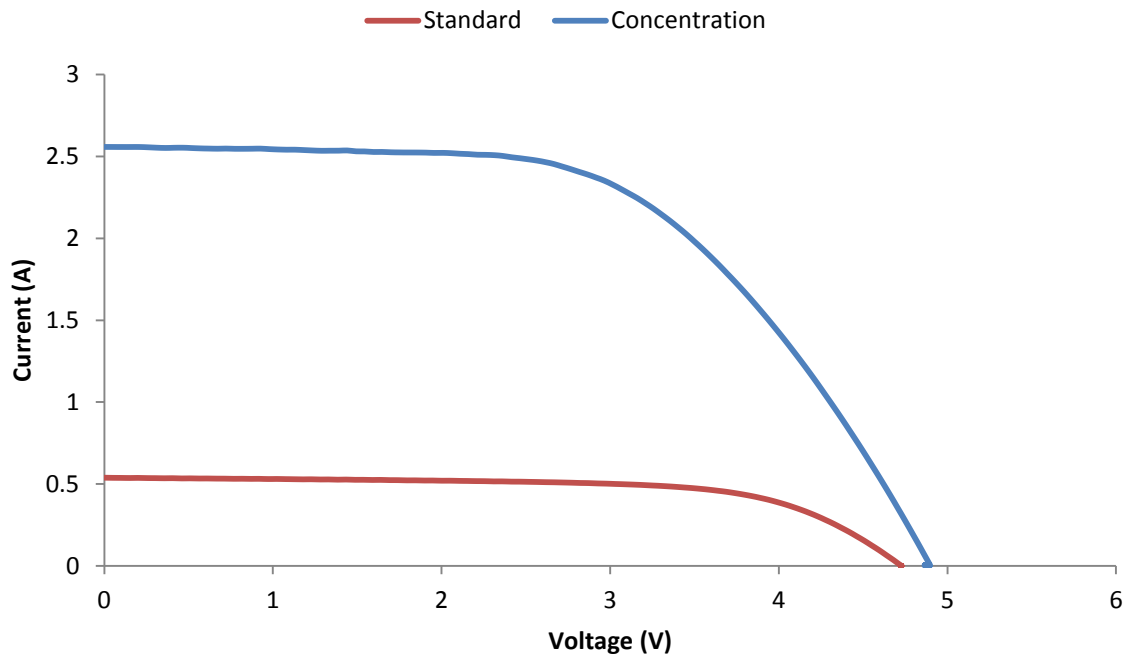


Figure 4.16: I-V characteristic of 8-cell PV receiver under 1-sun and 4.83-sun conditions

Table 4.3: I-V parameters and effective concentration ratio of the 4-, 6- and 8-cell receivers

	4-Cell	
	1-Sun	4.83-Sun
$I_{sc}$	1.13 A	5.28 A
$V_{oc}$	2.28 V	2.43 V
$P_{max}$	1.62 W	5.78 W
$X_E$	4.67	
	6-Cell	
	1-Sun	4.83-Sun
$I_{sc}$	0.72 A	3.38 A
$V_{oc}$	3.51 V	3.61 V
$P_{max}$	1.48 W	6.50 W
$X_E$	4.69	
	8-Cell	
	1-Sun	4.83-Sun
$I_{sc}$	0.54 A	2.56 A
$V_{oc}$	4.73 V	4.88 V
$P_{max}$	1.67 W	7.13 W
$X_E$	4.74	

In general, the short circuit current of each PV receiver increased by a factor approximately equal to the concentration ratio as predicted by Equation 4.8, while the open circuit voltage increased only slightly as predicted by Equation 4.9. The effective concentration ratio is of the order of 4.7, which corresponds well with the geometric concentration ratio of 4.83 as discussed in Chapter 3. A loss of only 2.5% is thus associated with the optical sub-system and indicates satisfactory optical sub-system design.

## **4.4 Summary**

Smaller, low current, PV cells are capable of reducing the power losses associated with series resistance under concentration. The experimental 8-cell PV receiver had a maximum power point of 7.13W, which corresponds to a 23% improvement compared to the 4-cell PV receiver. These results indicate that the use of low current PV cells is necessary to minimize the effect of series resistance and to consequently maximize the power produced under concentration. The following chapter investigates the various parameters and conditions that influence the temperature of a PV receiver within LCPV system. It also evaluates the use a thermal management system to limit the temperature of the PV receiver.

## 4.5 References

- [1] Lorenzo, E; *Solar Electricity: Engineering of Photovoltaic Systems*, Progensa, 1994.
- [2] Luque, A, Hegedus, S; *Handbook of Photovoltaic Science and Engineering*; John Wiley & Sons, 2011.
- [3] Andreev, VM, Grilikhes, VA, Rumiāntsev, VD; *Photovoltaic Conversion of Concentrated Sunlight*; John Wiley, 1997.
- [4] Luque, A, Hegedus, S; *Handbook of Photovoltaic Science and Engineering*; John Wiley & Sons, 2011.
- [5] EQ Macabebe, Investigation of device and performance parameters of photovoltaic devices, PhD Thesis, Nelson Mandela Metropolitan University, 2010.
- [6] Hatwaambo, S; *Performance Analysis of Low Concentrating PV-CPC Systems with Structured Reflectors* (University of Zambia); Internet: [http://cdn.intechopen.com/pdfs/28486/InTech-Performance\\_analysis\\_of\\_low\\_concentrating\\_pv\\_cpc\\_systems\\_with\\_structured\\_reflectors.pdf](http://cdn.intechopen.com/pdfs/28486/InTech-Performance_analysis_of_low_concentrating_pv_cpc_systems_with_structured_reflectors.pdf) (Accessed: 17 July 2012).
- [7] Alimardani,A, Afzali-Kusha, A; *Simulation and Optimization of Ga<sub>x</sub>In<sub>1-x</sub>P Cells for Concentrated Sunlight*, (University of Tehran); Internet: [http://ases.conference-services.net/resources/252/2859/pdf/SOLAR2012\\_0095\\_full%20paper.pdf](http://ases.conference-services.net/resources/252/2859/pdf/SOLAR2012_0095_full%20paper.pdf) (Accessed: 3 November 2012).
- [8] McEvoy, A, Markvart, T, Castaner, L ; *Practical Handbook of Photovoltaics: Fundamentals and Applications*; Academic Press, 2011.
- [9] Younis M.A; *Theoretical Investigation Of the Efficiency Of Silicon Solar Cell*; M.SC. Thesis, University of Musol, College Of Engineering, 1985.
- [10] Effect of Light Intensity. [s.a.]. Internet: <http://www.pveducation.org/pvcdrom/solar-cell-operation/effect-of-light-intensity> (Accessed: 25 June 2012)
- [11] RS Components. [s.a.]. Internet: <http://za.rs-online.com/web/p/thermally-conductive-insulators/3293299/> (Accessed: 9 March 2012)
- [12] MA Benecke, *On the Optical and Electrical Design of LCPV Modules*, MSc Thesis, Nelson Mandela Metropolitan University, 2012.

# Chapter 5

## THERMAL SUB-SYSTEM

Efficient thermal management is an essential component of LCPV system design. The high temperatures associated with a LCPV system significantly reduces the maximum power produced. The PV cells used in LCPV systems are also placed under high thermal stress which may result in degradation. This chapter outlines the development of a thermal model aimed at quantifying the energy absorbed and dissipated by various mechanisms in a LCPV system. The effect of environmental conditions, such as irradiance and wind velocity, on PV receiver temperature is also investigated. The benefits of a heat sink are investigated and the chapter is concluded with a thermal stress evaluation.

## 5.1 Temperature Effects

The high temperatures associated with LCPV systems significantly reduce the maximum power of the LCPV system. The reduction in power is predominantly attributed to the decrease of voltage as the temperature increases.

### 5.1.1 Intrinsic Carrier Concentration

The saturation current ( $I_{o1}$ ), as discussed in Chapter 4, is proportional to the intrinsic carrier concentration ( $n_i$ ) of the semiconductor material [1].

$$I_{o1} \propto n_i \quad (5.1)$$

The intrinsic carrier concentration is, however, dependent on temperature and may be calculated by the following equation [1]:

$$n_i = 2(m_n m_p)^{3/4} \left( \frac{2\pi kT}{h^2} \right)^{3/2} e^{-E_G/2kT} \quad (5.2)$$

$m_n$  and  $m_p$  are the masses of electrons and holes respectively.  $k$  is the Boltzmann constant and  $h$  is Planck's constant.  $T$  is temperature and  $E_G$  is the band gap.

The temperature dependence described by Equation 5.2 consequently leads to an increase in the saturation current as temperature increases. In addition, temperature dependent band gap narrowing also increases the intrinsic carrier concentration as temperature increases. The following equation describes the band gap of a semiconductor as a function of temperature [1]:

$$E_G = E_{G0} - \frac{\alpha T^2}{T + \beta} \quad (5.3)$$

$E_{G0}$  is the band gap at absolute zero.  $\alpha$  and  $\beta$  are constants specific to the semiconductor material.

Consequently, the band gap of a semiconductor decreases significantly when the temperature increases and thus the intrinsic carrier concentration is expected to increase in accordance with Equation 5.2. Figure 5.1 shows simulated I-V characteristics at high (70°C) and low (20°C) temperatures.

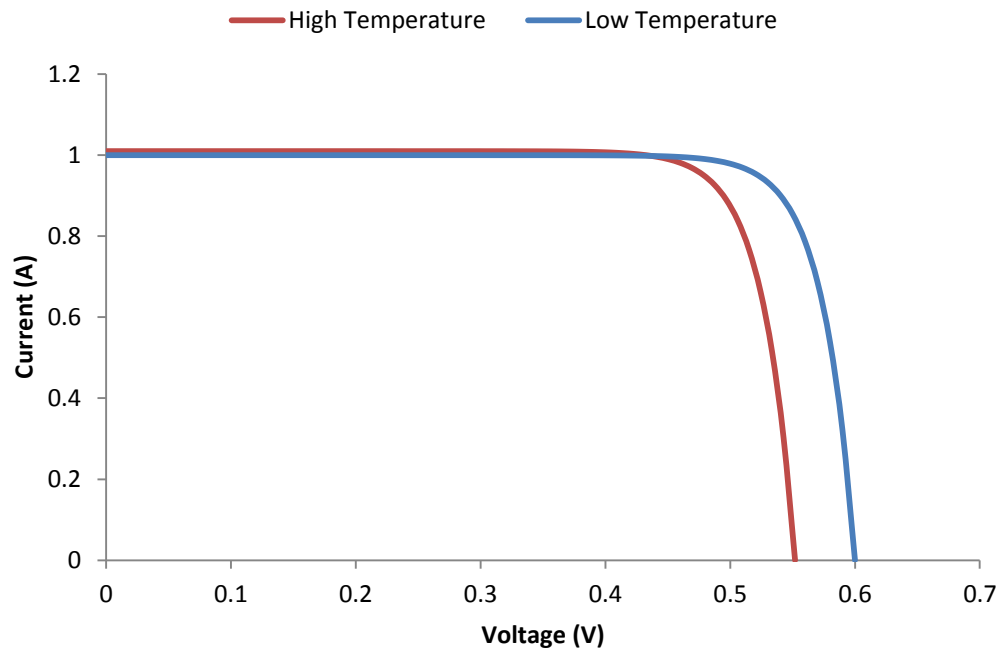


Figure 5.1: Simulated I-V characteristics showing the effect of temperature

### 5.1.2 Open Circuit Voltage

Equation 5.4 suggests that an increased saturation current would decrease the open circuit voltage.

$$V_{oc} = kT/q \ln \left( I_{sc}/I_{01} + 1 \right) \quad (5.4)$$

Equation 5.4 may also be re-arranged to solve for short circuit current:

$$I_{sc} \approx I_{01} e^{qV_{oc}/kT} \quad (5.5)$$

However, short circuit current is only slightly dependant on temperature and this dependence may be neglected under typical operating conditions such that [1]:

$$\frac{dI_{sc}}{dT} = 0 \quad (5.6)$$

Alternatively, differentiating Equation 5.3 yields:

$$\frac{dV_{oc}}{dT} = \frac{E_{G0}/q - V_{oc} + \xi kT/q}{T} \quad (5.7)$$

$\xi$  is a function of temperature.

For silicon at 300K, Equation 5.7 corresponds to approximately -2.3mV/°C [2]. Typically, an increase in temperature significantly decreases the open circuit voltage, while the short circuit current only increases slightly as shown in Figure 5.1. The overall result is a noticeable decrease of maximum power (-0.4%/°C).

## 5.2 Thermal Model

The development and experimental evaluation of a thermal model is necessary to fully understand the energy transfer mechanisms associated with a LCPV system. The thermal model may then be used to predict the operating temperatures and assess the thermal management requirements of the LCPV system.

### 5.2.1 Development

The thermal model is based on the principle of conservation of energy [3], which states that energy may never be created or destroyed, only transformed. A LCPV system has only one form of incident energy, namely irradiance. However, the LCPV system may dissipate energy in various ways, including convection, radiation and electrical work. A small amount of energy may also be lost through reflection from the PV cell surface. Owing to the anti-reflective property of PV cells, energy lost through reflection is assumed to be negligible. Figure 5.2 shows the energy absorbed and dissipated in a LCPV system.

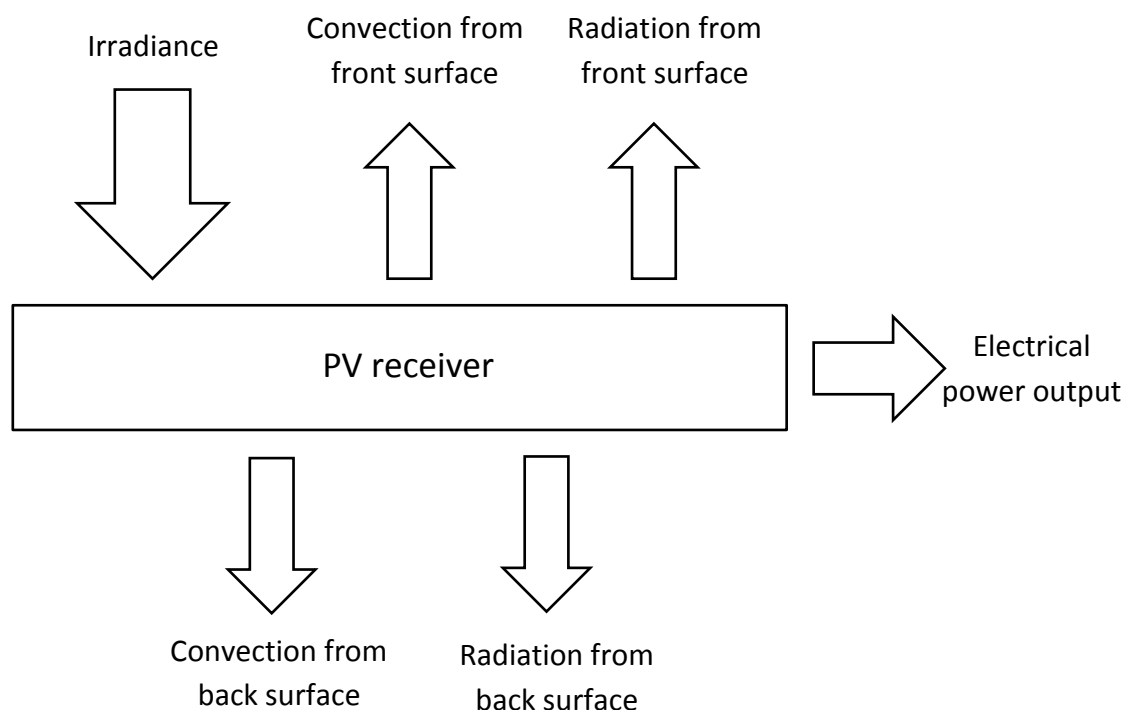


Figure 5.2: Energy absorption and dissipation in a LCPV system

The energy absorbed and dissipated in a LCPV system may be described by the following equations:

$$Q_A = Q_i \quad (5.8)$$

$$Q_D = Q_c + Q_r + Q_e \quad (5.9)$$

$Q_A$  is the total energy absorbed per unit time and  $Q_D$  is the total energy dissipated per unit time. The parameters  $Q_i$ ,  $Q_c$ ,  $Q_r$  and  $Q_e$  represent the energy absorbed and dissipated per unit time through concentrated irradiance, convection, radiation and electrical power output, respectively.

$Q_i$ ,  $Q_c$ ,  $Q_r$  and  $Q_e$  may be determined by the following equations:

$$Q_i = X\tau A \quad (5.10)$$

$$Q_c = Ah(T_m - T_a) \quad (5.11)$$

$$Q_r = A\varepsilon\sigma(T_m^4 - T_a^4) \quad (5.12)$$

$$Q_e = VI \quad (5.13)$$

$X$  is the concentration factor associated with the LCPV system and  $\tau$  is the direct irradiance.  $A$  is the area of the PV receiver.  $h$  is the convective transfer co-efficient.  $T_m$  is the PV receiver temperature and  $T_a$  is the ambient temperature.  $\varepsilon$  and  $\sigma$  are the emissivity of the PV receiver and Stefan-Boltzmann constant, respectively.  $V$  is the voltage over the electrical load and  $I$  is the current flowing through the electrical load.

Under certain conditions, such as constant irradiance and ambient temperature, the PV receiver temperature should remain relatively constant over a period of time. This indicates that the LCPV system has reached steady state conditions. During steady state conditions the energy absorbed must be equal to the energy dissipated.

For this reason, under steady state conditions:

$$Q_A = Q_D \quad (5.12)$$

$$Q_i = Q_c + Q_r + Q_e \quad (5.14)$$

$$X\tau A = Ah(T_m - T_a) + A\varepsilon\sigma(T_m^4 - T_a^4) + VI \quad (5.15)$$

Equation 5.15 is the driving relationship behind all thermal analysis in this chapter.

Owing to the high thermal conductivity of the materials used, the temperature of the front surface of the PV receiver is assumed to be equal to the temperature of the back surface of the PV receiver. The emissivity of the aluminium used in the PV receiver design is 0.8. The emissivity of a solar cell is generally greater than 0.8 [9]. The emissivity of the entire PV receiver is therefore assumed to be 0.8.

## 5.2.2 Validation

An experiment was designed to validate the thermal model described in 5.1.1. The objective of the experiment was to quantify the energy absorbed and dissipated. For the thermal model to be validated the energy dissipated would need to be equal to the energy absorbed.

### 5.2.2.1 Convective Transfer Co-efficient

All parameters of the thermal model, as described by equation 5.15, can be easily determined or measured, except the convective transfer co-efficient  $h$ . The convective transfer co-efficient is dependent on the geometry of the system (eg. vertical or horizontal air flow) and various other air properties such as air flow velocity and viscosity. The following equation can be used to determine the convective transfer co-efficient [4] for laminar air flow over a flat horizontal plate:

$$h = \overline{Nu}k_0/L \quad (5.16)$$

$k_0$  is the thermal conductivity of air and  $L$  is the length of the plate in the direction of air flow.  $\overline{Nu}$  is the average Nusselt number and can be determined by the following equation:

$$\overline{Nu} = 0.664Re^{1/2}Pr^{1/3} \quad (5.17)$$

$Re$  is the Reynolds number and  $Pr$  is the Prandtl number. Equation 5.17 is valid when  $Pr \geq 0.6$ .  $Re$  and  $Pr$  can be determined by the following equations:

$$Re = vL/\omega \quad (5.18)$$

$$Pr = \omega/\alpha \quad (5.19)$$

$v$  is the velocity of the air flow and  $L$  is the length of the plate in the direction of air flow.  $\omega$  is the kinematic viscosity and  $\alpha$  is the thermal diffusivity.

The complex and dynamic geometry associated with a 2-axis tracker mounted LCPV system and the high dependence on environmental conditions makes calculation of the convective transfer coefficient complicated [5]. For this reason, it is advantageous to calculate the convective transfer coefficient by considering the change in air temperature across the PV receiver. The energy absorbed by the air is equivalent to the energy dissipated by the PV receiver through convection. The energy dissipated through convection may thus be calculated by the following equation:

$$Q_c = \dot{m}C(T_{out} - T_{in}) \quad (5.19)$$

$\dot{m}$  is the air mass flow rate.  $C$  is the specific heat capacity of air.  $T_{out}$  is the temperature of the air after passing over the PV receiver and  $T_{in}$  is the ambient temperature.

The convective transfer co-efficient may then be calculated by the following equation:

$$h = Q_c / A\Delta T \quad (5.20)$$

$\Delta T$  is the temperature difference between the PV receiver and the ambient air and  $A$  is the area of the PV receiver.

### 5.2.2.2 Experimental

The LCPV system, consisting of the 7 facet reflector and a 6-cell PV receiver, was housed in an insulated wooden box to restrict energy transfer with the environment. This creates a control volume insulated from the environment in which the thermal model could be validated. Two panel fans were used to simulate air flow of 1.2 m/s across the PV receiver. Two glass sheets were mounted within the wooden box to ensure direct and parallel air flow. The mass flow rate ( $\dot{m}$ ) was approximately 0.05 kg/s. Figure 5.3 shows a simplified illustration of the thermal model validation experiment.

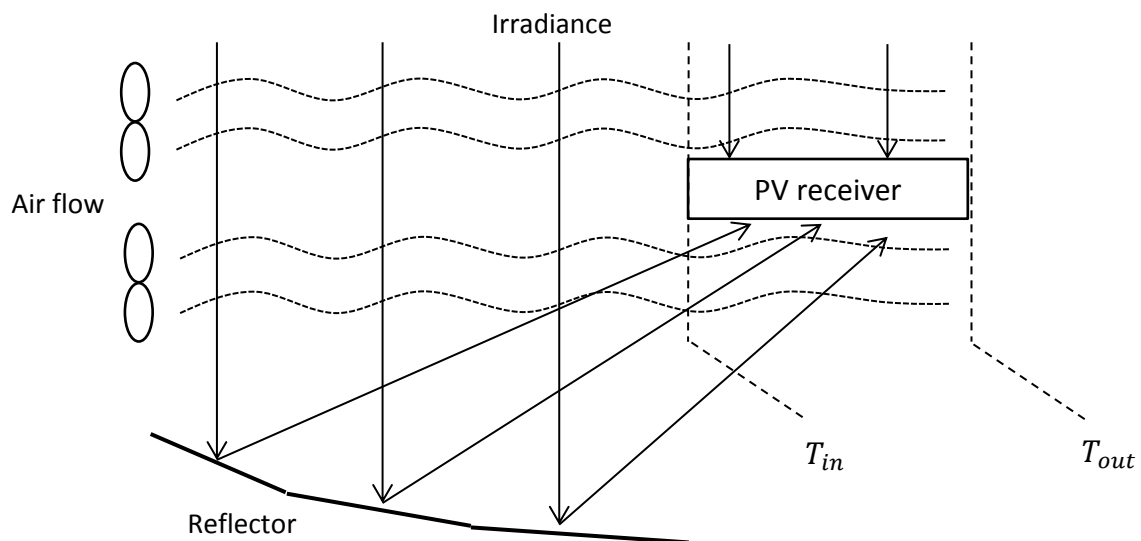


Figure 5.3: Thermal model validation experimental setup

Owing to reflective losses associated with the glass sheets, the concentration factor ( $X$ ) could not be calculated directly from the results discussed in Chapter 4. Instead, the concentration factor needed to be calculated through the reflectance of glass as described by the following Fresnel equations [6]:

$$\begin{aligned}
 R_1 &= \left[ \frac{n_1 \cos(\theta_i) - n_2 \cos(\theta_t)}{n_1 \cos(\theta_i) + n_2 \cos(\theta_t)} \right]^2 \\
 R_2 &= \left[ \frac{n_2 \cos(\theta_i) - n_1 \cos(\theta_t)}{n_2 \cos(\theta_i) + n_1 \cos(\theta_t)} \right]^2 \quad (5.21)
 \end{aligned}$$

$R_1$  is the reflectance when light is polarised perpendicular to the plane of incidence, while  $R_2$  is the reflectance when light is polarised parallel to the plane of incidence.  $n_1$  is the refractive index of the medium before the refractive interface is reached and  $n_2$  is the refractive index of the medium after the refractive interface. The refractive index of air and glass is assumed to be 1 and 1.5 respectively.  $R_1$  and  $R_2$  should be averaged in the case of unpolarised light. As shown in figure 5.3, the front and back surfaces of the PV receiver receive irradiance and a combined concentration factor of 4.48 was calculated.

Four K-type thermocouples were used to measure air temperatures within the LCPV system. An additional K-type thermocouple was used to measure PV receiver temperature.

The LCPV system was mounted on a two-axis tracker. The PV receiver was operated in open circuit, thus  $Q_e = 0$ . The experiment was conducted on a clear day in January 2012 and measurements were averaged over 2-minute intervals. The experiment was conducted for 1 hour.

### 5.2.2.3 Results

Figure 5.4 shows various system temperatures and irradiance over the experimental period. The PV receiver temperature was relatively constant over the last 10 data points, corresponding to the last 20 minutes of the experiment. The last 10 data points thus indicated steady state conditions and were averaged to perform the validation analysis of the thermal model. Quantification of these averaged values is shown in Table 5.1.

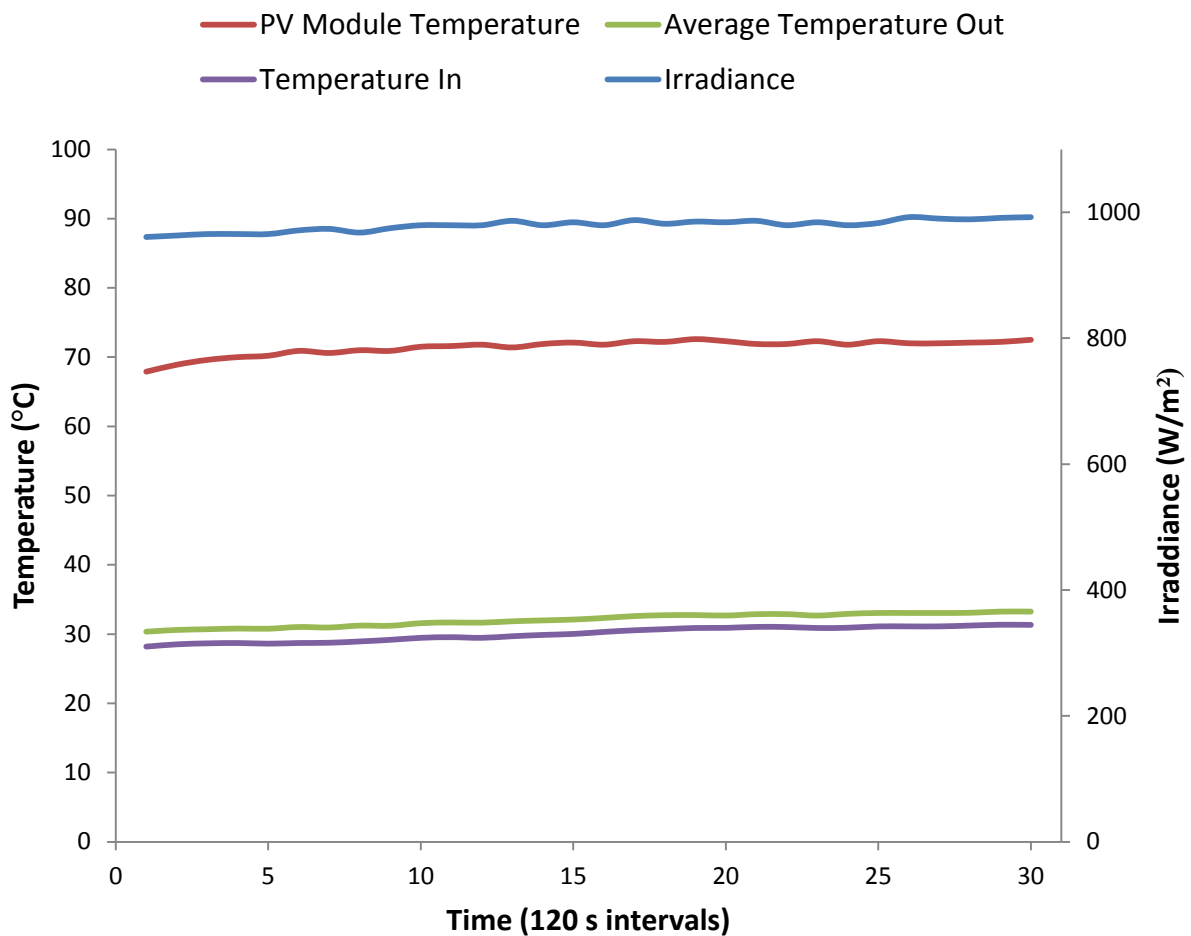


Figure 5.4: Graph showing irradiance and various LCPV system temperatures

Table 5.1: Thermal model validation analysis

Irradiance	987±6 W/m <sup>2</sup>
Concentration Factor	4.48
PV Receiver Area	0.025±0.001 m <sup>2</sup>
Total incident power	111±5 W
PV Cell temperature	72.0±0.2°C
Radiation power dissipated	13±0.1 W
Temperature In ( $T_{in}$ )	31.1±0.2°C
Temperature Out ( $T_{out}$ )	33.0±0.3°C
Air temperature difference	1.9±0.3°C
Air flow velocity	1.2±0.05 m/s
Convection power dissipated	101±18 W
Total dissipated power	113±18 W

The total dissipated power corresponds to the total incident power within measurement uncertainty. Despite the high uncertainty of the total power dissipated, the shaded values in Table 5.1 are still within the same order, suggesting that the thermal model will be an effective method of estimating the operating temperatures of a LCPV system. A convective transfer co-efficient of  $49\pm 9$  W/m<sup>2</sup>.K corresponds to the data listed in Table 5.1. However, the convective transfer co-efficient should be re-calculated using steady state data points at the beginning of each new experimental configuration due to its high dependence on environmental conditions and geometrical orientation. The thermal model allows convenient empirical calculation of the convective transfer co-efficient in the following sections of this chapter.

## 5.3 Environmental Conditions

It is clear from the thermal model that environmental factors, such as irradiance, wind velocity and ambient temperature, would impact PV receiver temperatures within a LCPV system. A series of experiments were conducted to analyse the effect of these environmental factors on PV receiver temperatures. The solve function in Mathematica was used to predict the PV receiver temperature in accordance with the thermal model. The user inputs irradiance and ambient temperature and the solve function calculates the predicted PV receiver temperature according to Equation 5.15. As mentioned before, the convective transfer co-efficient needs to be re-calculated at the beginning of each new experimental configuration and the model should then be adjusted accordingly.

### 5.3.1 Irradiance

Different irradiance conditions should not have any observable effect on the convective transfer co-efficient of the LCPV system at constant temperatures. Varying irradiance only disrupts the energy balance described by the thermal model. An increase in irradiance should result in higher PV receiver temperatures, while a decrease in irradiance should result in lower PV receiver temperatures. The relevant terms in equation 5.15 are highlighted below.

$$X \quad \tau \quad A = Ah \left( \underbrace{T_m}_{increase} - T_a \right) + A\epsilon\sigma \left( \underbrace{T_m^4}_{increase} - T_a^4 \right) + VI$$

#### 5.3.1.1 Experimental

The LCPV system was housed within the same insulating enclosure and two panel fans provided air flow of 1.2m/s as described in section 5.1.2.2. A K-type thermocouple was used to measure PV receiver temperature. Irradiance screens were placed over the LCPV system at various times throughout the experiment to decrease the irradiance incident on the PV receiver.

The LCPV system was mounted on a two-axis tracker. The PV receiver was operated in open circuit, thus  $Q_e = 0$ . The experiment was conducted on a clear day in February 2012 and measurements were averaged over 2-minute intervals. The experiment was conducted for 3 hours 20 min.

### 5.3.1.2 Results

Figure 5.5 shows the PV receiver temperature under varying irradiance conditions. It clearly illustrates the dependence of receiver temperature on irradiance. The PV receiver temperature is approximately 75°C when the irradiance is above 900 W/m<sup>2</sup>. However, the PV receiver temperature decreases significantly to approximately 45°C when the irradiance drops to below 300 W/m<sup>2</sup>. A convective transfer co-efficient of 43 W/m<sup>2</sup>.K was calculated according to Equation 5.15 for this experimental configuration. As can be seen from Figure 5.5, the thermal model predicts temperatures that correspond closely to the measured temperatures. The only noticeable errors associated with the thermal model occur as the irradiance is changed. These errors are unavoidable as thermal model assumes steady state conditions and does not take into account the time taken for the PV receiver to reach steady state conditions. In general, the thermal model predicts temperatures that are within 2% of the measured temperatures.

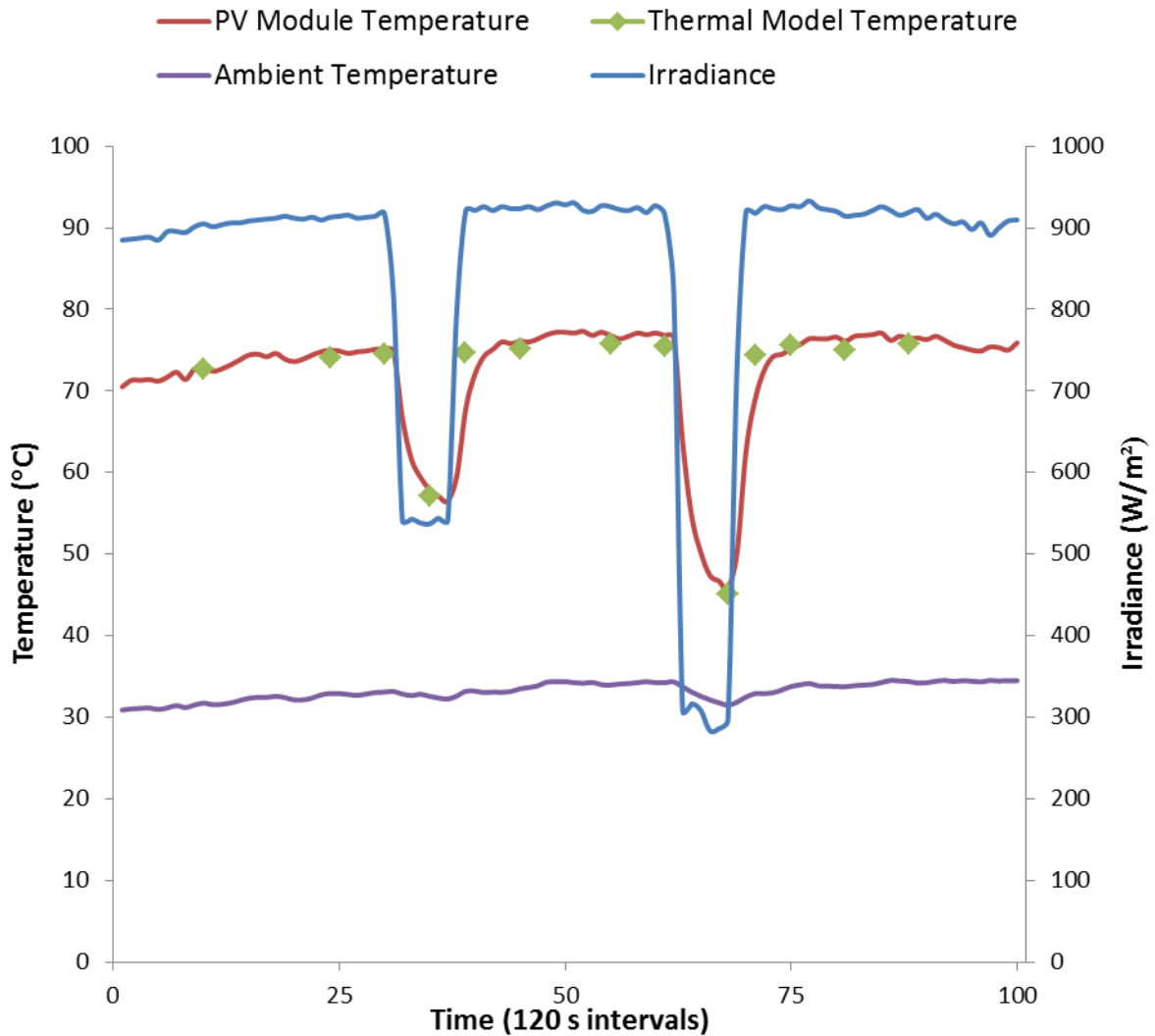


Figure 5.5: Graph showing dependence of PV receiver temperature on irradiance

### 5.3.2 Wind Velocity

Theoretically, the convective transfer co-efficient is dependent on the air velocity over the surface. According to equations 5.15, 5.16 and 5.17,  $h \propto v^{1/2}$  for laminar air flow over a horizontal plate. A higher wind velocity should result in a higher convective transfer co-efficient and subsequently a lower PV receiver temperature according to the thermal model. The relevant terms in equation 5.15 are highlighted below.

$$X\tau A = A \underbrace{h}_{\text{increase}} \left( \overbrace{\widehat{T}_m}^{\text{decrease}} - T_a \right) + A\epsilon\sigma \left( \overbrace{\widehat{T}_m^4}^{\text{decrease}} - T_a^4 \right) + VI$$

### 5.3.2.1 Experimental

The LCPV system was housed within the same insulating enclosure as described in Section 5.1.2.2. A K-type thermocouple was used to measure PV receiver temperature.

The LCPV system was mounted on a two-axis tracker. The PV receiver was operated in open circuit, thus  $Q_e=0$ . The experiment was conducted on a clear day in January 2012 and measurements were averaged over 2-minute intervals. The experiment was conducted for 4 hours.

### 5.3.2.2 Results

Figure 5.6 shows the PV receiver temperature as the air velocity was decreased periodically throughout the experiment. The PV receiver temperature is approximately 70°C when the air velocity is 1.2 m/s. However, the PV receiver temperature increases significantly to approximately 90°C when the air velocity is reduced to 0.6 m/s. For each air velocity a separate convective transfer co-efficient was calculated and the thermal model was adjusted accordingly. The convective transfer co-efficient corresponding to each air velocity is shown in Table 5.2.

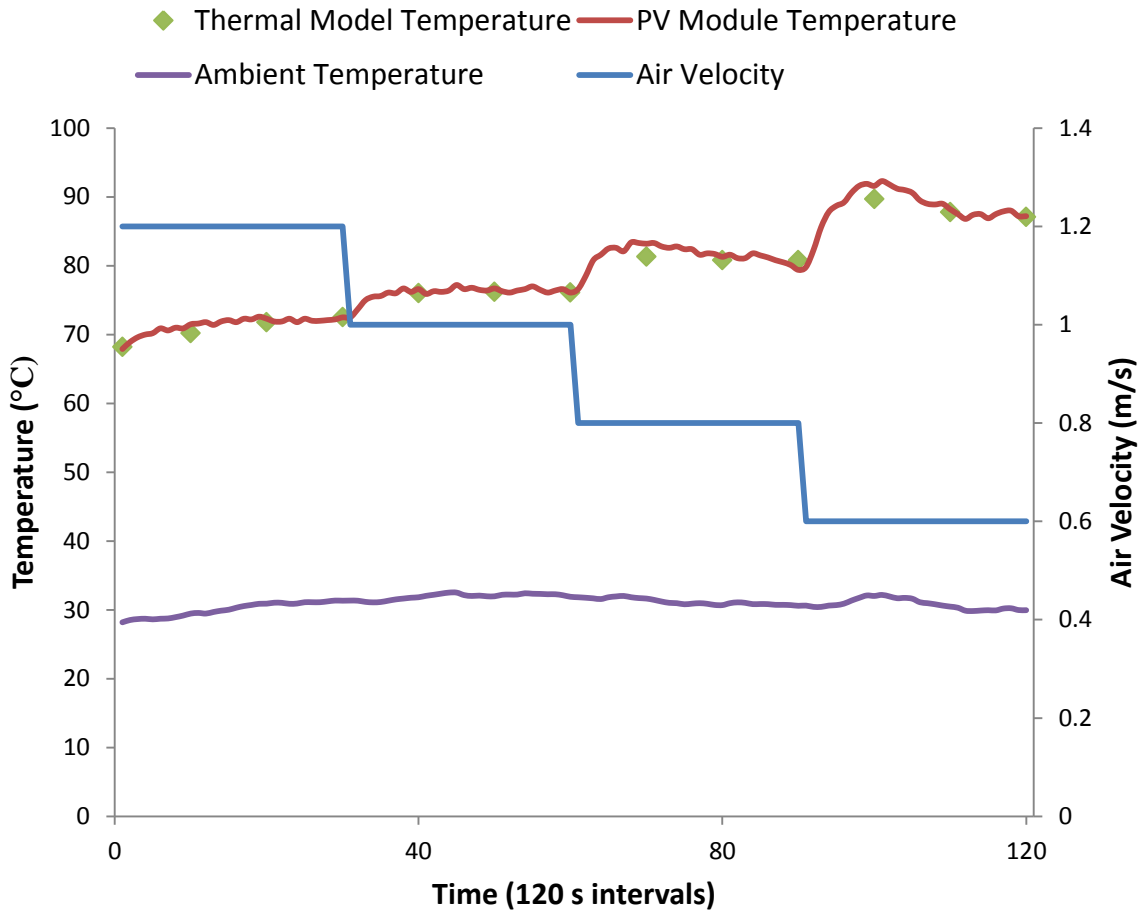


Figure 5.6: Graph showing the dependence of PV receiver temperature on air velocity

Table 5.2: Convective transfer co-efficient calculation

Air velocity	Convective transfer co-efficient
1.2 m/s	47.9 W/m <sup>2</sup> .K
1.0 m/s	44.0 W/m <sup>2</sup> .K
0.8 m/s	38.5 W/m <sup>2</sup> .K
0.6 m/s	32.7 W/m <sup>2</sup> .K

With reference to equations 5.16 - 5.19, it may be assumed that the convective transfer coefficient has the form  $h = h_0 v^c$ . The value of  $c$  may be determined graphically by the gradient of the  $\log(v)$  vs.  $\log(h)$  graph as shown in Figure 5.7.

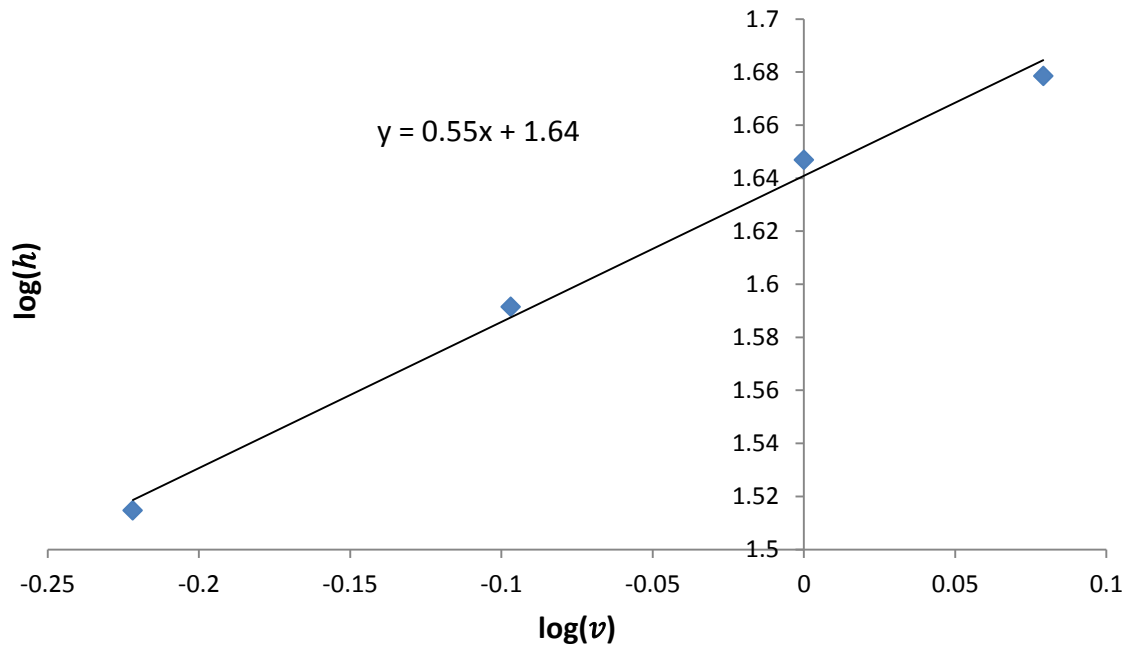


Figure 5.7:  $\log(v)$  vs.  $\log(h)$  graph corresponding to data in Table 5.2

According to Figure 5.7, the data in Table 5.2 corresponds to a  $c$  value of approximately 0.55. The relationship  $h = h_0 v^{0.55}$  corresponds closely to the theoretical relationship of  $h = h_0 v^{0.5}$  for laminar flow over a horizontal plate.

### 5.3.3 Ambient Temperature

A dedicated experiment to evaluate the effect of ambient temperature on PV receiver temperature was not conducted. Instead, the effect of ambient temperature was evaluated through the experiments focussing on irradiance and wind velocity. Considering Figures 5.4, 5.5 and 5.6, it is clear that PV receiver temperature is also strongly dependant on ambient temperature. PV receiver temperature increases as the ambient temperature increases. The reason for this behaviour can easily be explained through the thermal model as described by Equation 5.15. Assuming all other parameters, such as irradiance and convective transfer co-efficient, remain constant, the PV receiver temperature would need to increase as ambient temperature increased in order to maintain the energy balance. PV receiver temperature decreases as the ambient temperature decreases for the same reason. The relevant terms in equation 5.15 are highlighted below.

$$X\tau A = Ah \left( \underbrace{T_m}_{\text{increase}} - \underbrace{T_g}_{\text{increase}} \right) + A\varepsilon\sigma \left( \underbrace{T_m^4}_{\text{increase}} - \underbrace{T_a^4}_{\text{increase}} \right) + VI$$

## 5.4 Electrical Power

The effect of electrical power output has not yet been discussed or evaluated. However, it is clear from the thermal model that transformation of energy into electrical work would disrupt the energy balance. Energy dissipated from the LCPV system in the form of electrical power would result in less energy being dissipated by convection and radiation. The reduction of convection and radiation can only be achieved through a decrease of PV receiver temperature, assuming irradiance, ambient temperature and convective transfer co-efficient remain constant. For this reason, the PV receiver temperature should be lower when it performs electrical work. The relevant terms in equation 5.15 are highlighted below.

$$X\tau A = Ah \left( \overset{\text{decrease}}{\widetilde{T}_m} - T_a \right) + A\varepsilon\sigma \left( \overset{\text{decrease}}{\widetilde{T}_m^4} - T_a^4 \right) + \underset{\text{increase}}{VI}$$

### 5.4.1 Experimental

The LCPV system was housed within the same insulating enclosure as described in section 5.1.2.2. A K-type thermocouple was used to measure PV receiver temperature. Owing to spectral changes associated with the glass sheets used in the insulating enclosure, the maximum power output of the 6-cell PV receiver was reduced. In Chapter 4 the maximum power output of the 6-cell receiver was approximately 6.5 W. However, only 1 W was extracted by electrical work during this experiment.

The LCPV system was mounted on a two-axis tracker. The PV receiver was operated in open circuit ( $Q_e=0$ ) for 20 minutes. The PV receiver was then connected to a resistor, approximately matched to the maximum power point, to allow it to perform electrical work for 10 minutes. The PV receiver was operated in open circuit for the remainder of the experiment. The experiment was conducted on a clear day in February 2012 and measurements were averaged over 2-minute intervals. The experiment was conducted for 50 minutes. The irradiance was relatively constant throughout the experiment ( $900 \pm 20$  W/m<sup>2</sup>)

### 5.4.2 Results

Figure 5.8 shows the PV receiver temperature when electrical power is extracted. The energy balance is only slightly disrupted by the extraction of 1 W electrical power and the decrease in PV receiver temperature is only 2°C. However, the effect of electrical power extraction becomes more apparent when the difference between PV receiver temperature and ambient temperature is considered.

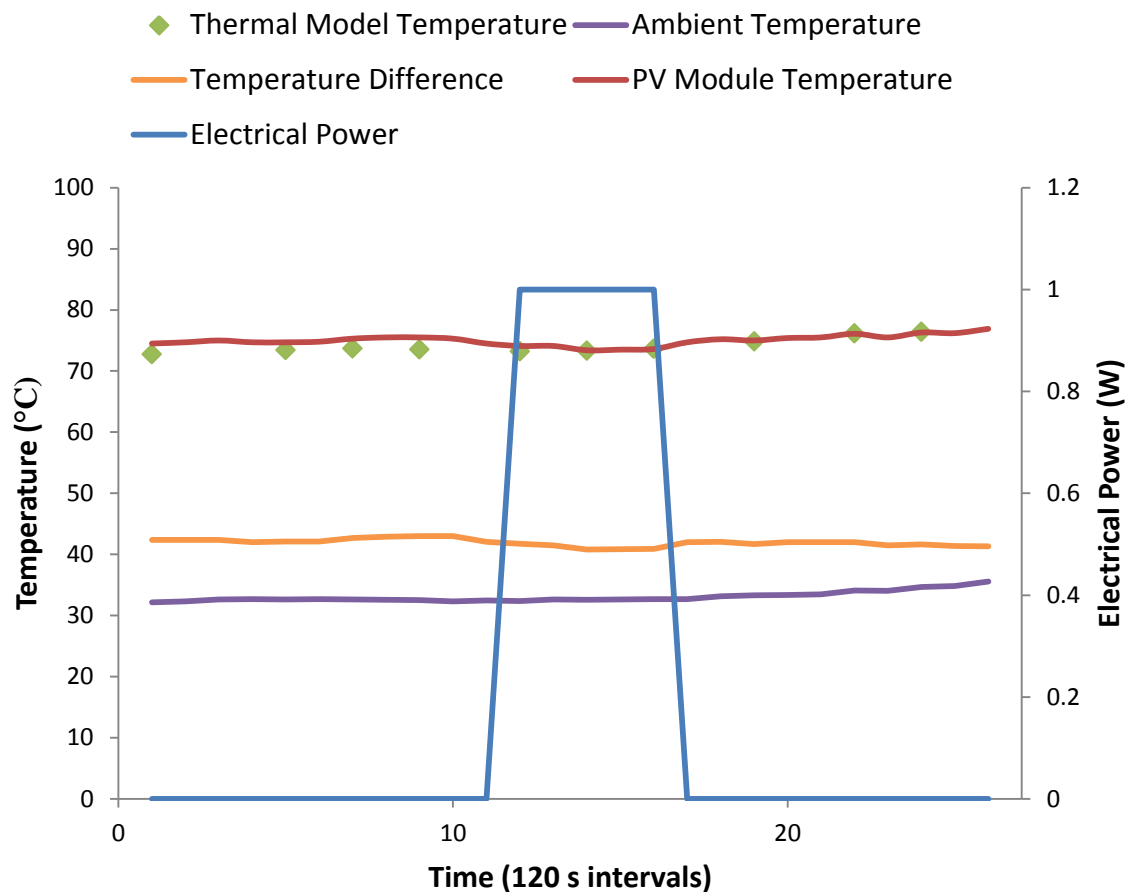


Figure 5.8: Graph showing PV receiver temperature when 1 W electrical power is extracted

According to the thermal model described by equation 5.15, the temperature difference should be constant when the irradiance, and all other parameters, is relatively constant. However, the temperature difference decreases slightly when electrical power is extracted, indicating that the energy balance has been disrupted. This observation is consistent with the thermal model.

The convective transfer co-efficient of  $42.9 \text{ W/m}^2\cdot\text{K}$  was calculated for this experiment. The thermal model once again predicts PV receiver temperatures that correspond closely to the experimental data. Figure 5.9 shows the predicted PV receiver temperature if 6.5 W of electrical power was extracted as measured in Chapter 4. The decrease in PV receiver temperature is much more significant when the electrical power extracted is greater.

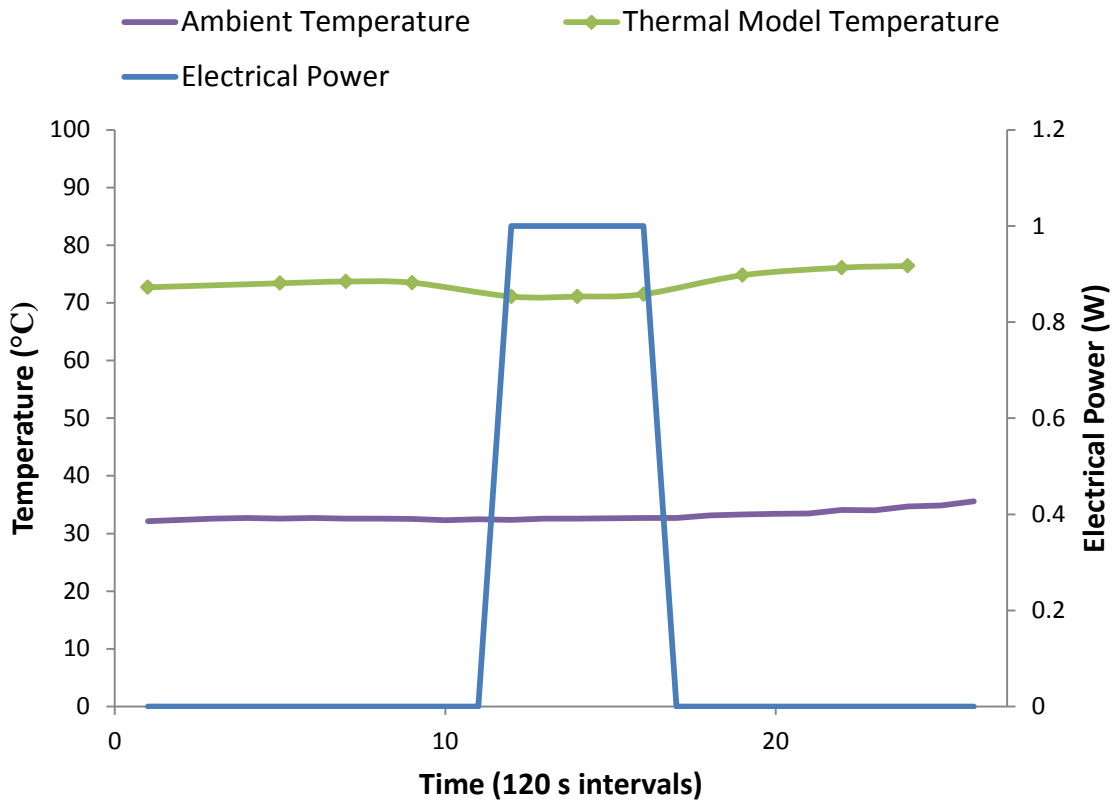


Figure 5.9: Graph showing modelled PV receiver temperature when 6.5 W electrical power is extracted

## 5.5 Heat Sink

The primary function of a heat sink in a LCPV system is to decrease the temperature of the PV receiver. This is achieved by providing a larger area for convection to occur. The relevant terms in equation 5.15 are highlighted below.

$$X\tau A = \underbrace{A}_{\substack{\uparrow \\ \text{increase}}} h \left( \overbrace{\widehat{T}_m}^{\text{decrease}} - T_a \right) + A\epsilon\sigma \left( \overbrace{\widehat{T}_m^4}^{\text{decrease}} - T_a^4 \right) + VI$$

### 5.5.1 Design

Figure 5.10 shows a basic illustration of the heat sink used in this study. The heat sink is manufactured from aluminium and has 25 fins. The convective area for the heat sink configuration is approximately 0.125 m<sup>2</sup>, while the convective area for the configuration without the heat sink is 0.05 m<sup>2</sup>.

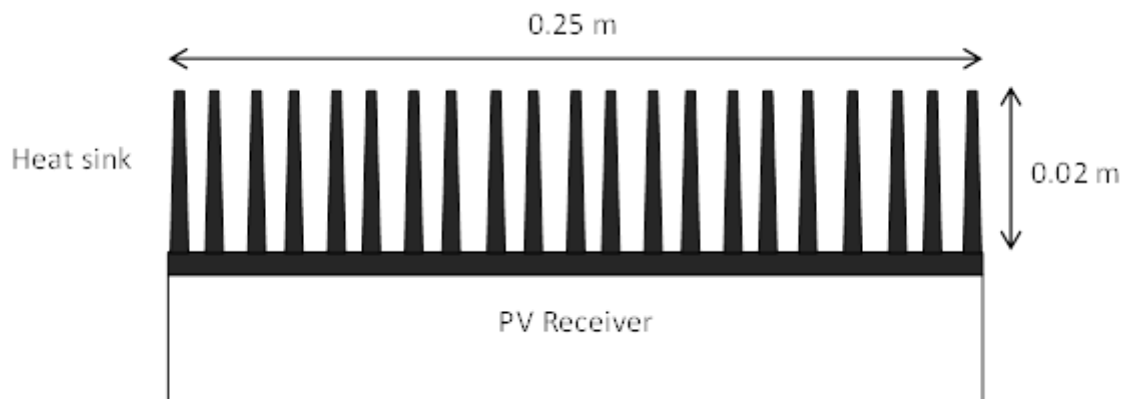


Figure 5.10: Simplified illustration of heat sink

Assuming that the irradiance is constant and that energy dissipated by radiation is unaffected, the energy dissipated through convection should be equal for both configurations.

$$A_1 h(T_{m1} - T_a) \approx A_2 h(T_{m2} - T_a) \quad (5.22)$$

$A_1$  is the convective area of the configuration without the heat sink, while  $A_2$  is the convective area of the configuration with the heat sink. Therefore,  $2.5A_1 = A_2$ .

The relationship may be further simplified by the assumption that the convective transfer co-efficient is unchanged by the introduction of a heat sink.

$$A_1 \Delta T_1 \approx A_2 \Delta T_2 \quad (5.23)$$

$$A_1 \Delta T_1 \approx 2.5A_1 \Delta T_2 \quad (5.24)$$

$$\Delta T_1 \approx 2.5\Delta T_2 \quad (5.25)$$

This basic theoretical analysis of both configurations shows that the temperature difference of the configuration without the heat sink is 2.5 times greater than the configuration with the heat sink.

Unfortunately, a heat sink is not 100% efficient. The fins of a heat sink have a finite length which gives rise to a temperature gradient along each fin. Practically, the tip of the fin has a lower temperature than the base of the fin. This results in non-uniform convection of energy along the fin.

The efficiency of a heat sink is given by the following equations [1]:

$$\eta = \tan(mL) / mL \quad (5.26)$$

$$mL = \sqrt{hP/kA} L \quad (5.27)$$

$h$  is the convective transfer co-efficient and  $k$  is the thermal conductivity of aluminium.  $P$  is the perimeter of the heat sink fin, but may be approximated as twice the fin width for a thin fin.  $A$  is the surface area of the heat sink fin and  $L$  is the length of the fin.

When the efficiency of the heat sink described above is computed, a value of 0.93 is obtained. Equation 5.22 should now be adjusted to include heat sink fin efficiency.

$$A_1 h(T_{m1} - T_a) \approx \eta A_2 h(T_{m2} - T_a) \quad (5.28)$$

$$\Delta T_1 \approx 2.325 \Delta T_2 \quad (5.29)$$

The inclusion of this type of heat sink in the LCPV system should reduce the difference between the PV receiver temperature and the ambient temperature by a factor 2.325.

### 5.5.2 Experimental

The LCPV system was housed within the same insulating enclosure as described in section 5.1.2.2. A K-type thermocouple was used to measure PV receiver temperature. Two panel fans were used to simulate air flow of 1.2m/s across the PV receiver. The LCPV system was mounted on a two-axis tracker. The PV receiver was operated in open circuit, thus  $Q_e=0$ .

The experiment was conducted on a two separate days in February 2012 and measurements were averaged over 2-minute intervals. The experiment was conducted for 50 minutes on each day. The irradiance was relatively constant during the experimental period on each day. The heat sink was attached to the PV receiver on the second day.

### 5.5.3 Results

Figure 5.11 shows the temperature difference between the PV receiver temperature and the ambient temperature. It is clearly illustrated in Figure 5.11 that the addition of the heat sink reduces the temperature difference. The temperature difference is approximately 40°C without a heat sink and approximately 25°C when a heat sink is included. Experimentally the temperature difference is reduced by a factor of 1.6, which is less than predicted by equation 5.25.

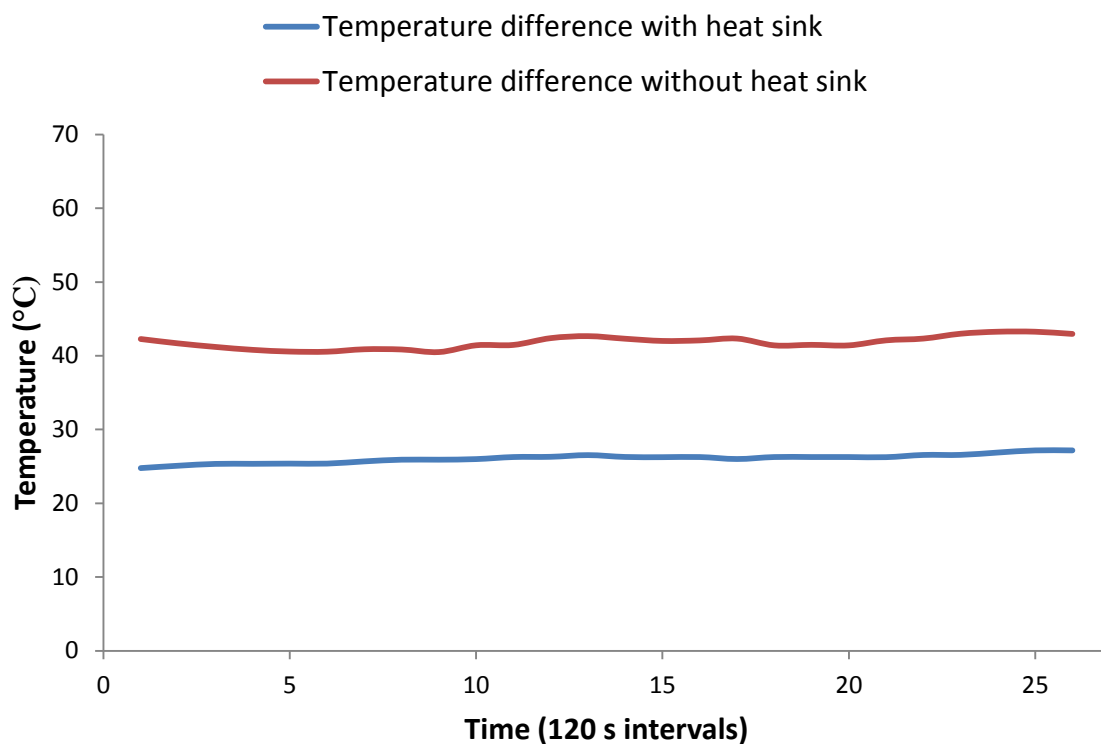


Figure 5.11: Graph showing temperature difference with/without heat sink

In section 5.4.1 it was assumed that the convective transfer co-efficient remains constant when the heat sink is attached to the PV receiver and only the convective area is increased. However, the heat sink fins may reduce the air velocity and consequently the convective transfer co-efficient would be less than expected as shown in section 5.2.2.2. Using the thermal model, a convective transfer co-efficient of 43W/m<sup>2</sup>.K was calculated for the configuration without a heat sink. Similarly, a convective transfer co-efficient of 32W/m<sup>2</sup>.K was calculated for the configuration with a heat sink. The addition of the heat sink, and the associated decrease in air velocity, causes the convective transfer co-efficient to decrease by approximately 25%.

## 5.6 Thermal Stress Evaluation

It is suspected that long term PV cell operation at high temperatures may lead to degradation and a subsequent reduction in power output. The following experiment was designed to assess the degradation, if any, of the PV cells after a period of thermal stress.

### 5.6.1 Experimental

The LCPV system was housed within the same insulating enclosure as described in section 5.1.2.2. A K-type thermocouple was used to measure PV receiver temperature. Two panel fans were used to simulate air flow of less than 0.5m/s across the PV receiver and no heat sink was attached to the PV receiver. The low air velocity and exclusion of a heat sink ensured that the PV cells were subjected to high operating temperatures. The LCPV system was mounted on a two-axis tracker. The PV receiver was operated in open circuit, thus  $Q_e=0$ .

The experiment was conducted on several clear days in March 2012 and measurements were averaged over 2-minute intervals. The experiment was conducted for approximately 35 hours in total. The total energy incident on the PV receiver during the experimental period was approximately 135kWh/m<sup>2</sup>. I-V characteristics of the PV receiver were measured before and after the experiment.

### 5.6.2 Results

Figure 5.12 shows the time of operation of the PV receiver as a function of operating temperature. The PV receiver operated at temperatures between 91°C and 100°C for approximately 25 hours. The PV receiver also operated at temperatures above 100°C for approximately 5 hours. As can be seen from Figure 5.11, the PV receiver operated at temperatures between 81°C and 110°C for more than 95% of the experimental period.

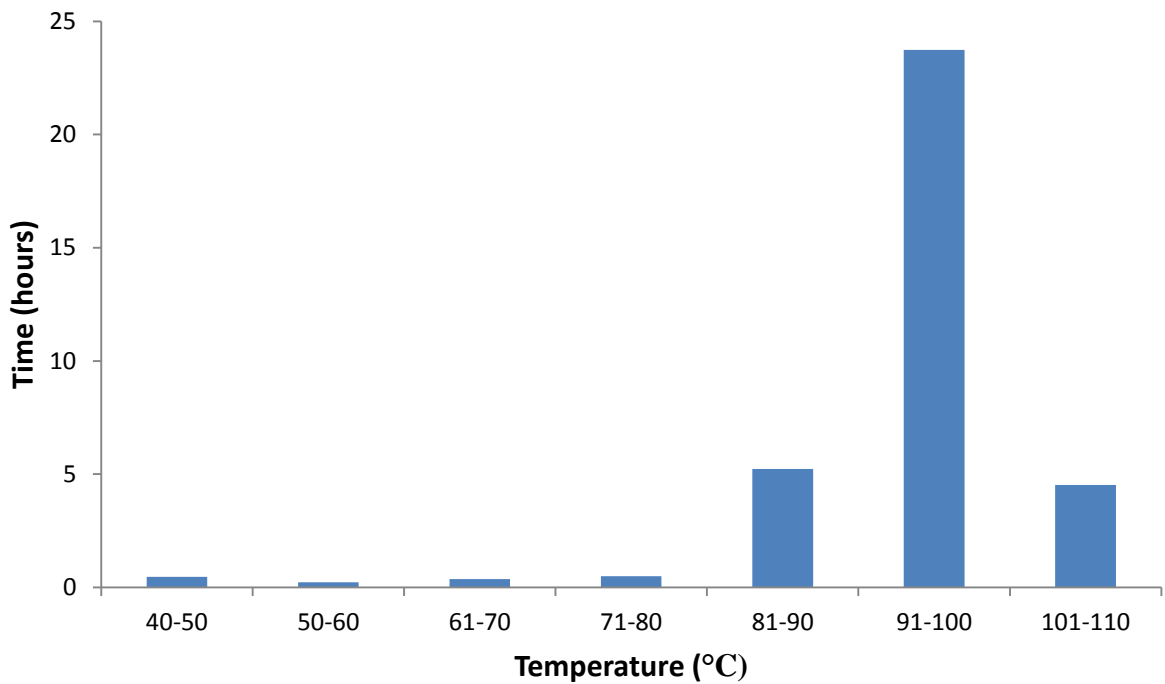


Figure 5.12: Graph showing the frequency of PV receiver operating temperatures

Figure 5.13 shows the IV characteristics under concentration conditions before and after the experimental period. Current was corrected to irradiance of  $1000 \text{ W/m}^2$  and voltage was corrected to temperature of  $25^\circ\text{C}$ . Short circuit current and maximum power point increased slightly after the period of thermal stress. The open circuit voltage decreased slightly after the period of thermal stress and the fill factor was unchanged after the period of thermal stress. Table 5.3 gives a summary of various parameters before/after thermal stress.

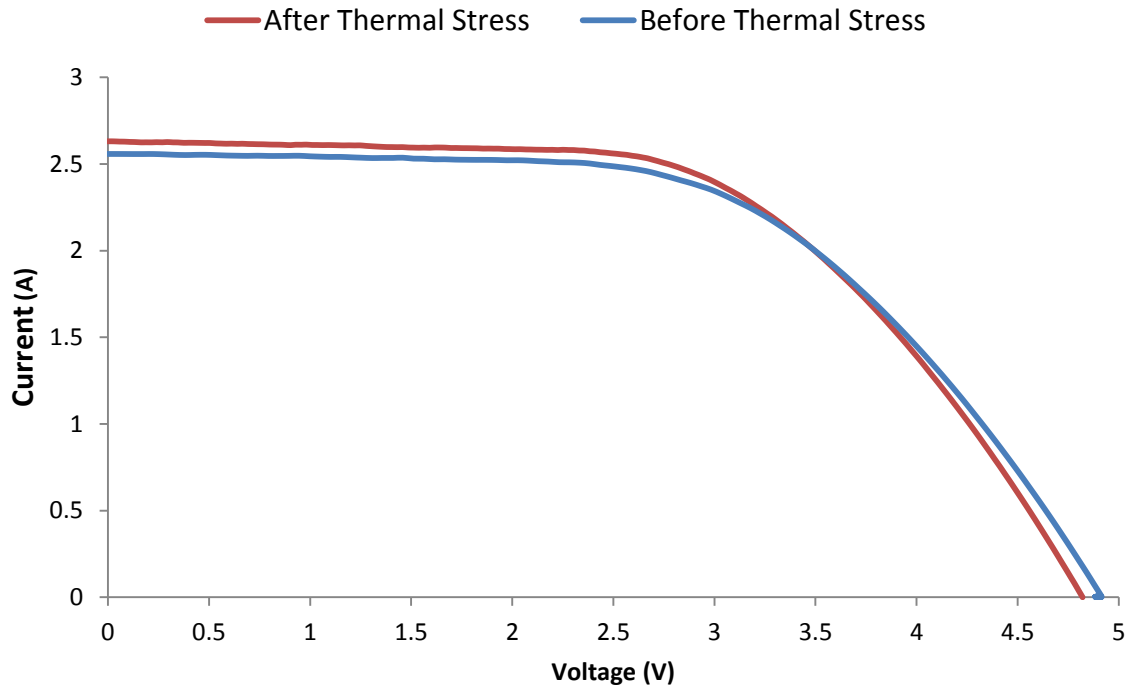


Figure 5.13: IV characteristics of the PV receiver under concentration conditions before/after thermal stress

Table 5.3: Various electrical parameters before/after thermal stress

	Before	After	$\Delta$ (%)
$I_{sc}$ (A)	2.56	2.63	2.7
$V_{oc}$ (V)	4.89	4.82	-1.4
$P_{max}$ (W)	7.15	7.24	1.3
$FF$	0.57	0.57	0
$X$	4.74	4.70	-0.8

Despite the small fluctuations, within measurement uncertainty, of the electrical parameters, it seems reasonable to conclude that the period of thermal stress did not have an apparent negative effect on the electrical performance of the LCPV system. It is thus possible that the polymer compounds, such as ethylene-vinyl-acetate (EVA) and Ethylene tetrafluoroethylene (ETFE), are responsible for the degradation of the PV receiver under thermal stress [7, 8]. Since no polymer compounds were used in this experiment it is expected that the PV receiver would not degrade under thermal stress.

## 5.7 Summary

The thermal model predicted temperatures that corresponded closely to the experimental equivalents under various operating conditions. The thermal model allows empirical calculation of the convective transfer co-efficient and may be used to predict operating temperatures of a LCPV system. Operating temperatures in excess of 90°C were recorded under experimental conditions, but the addition of heat sink reduced the temperature difference by a factor of 1.6. This value is significantly less than the theoretical value of 2.35, suggesting a decreased convective transfer co-efficient when the heat sink is attached. The high temperatures associated with a 35 hour thermal stress test did not significantly degrade the silicon PV cells used in this study.

## 5.8 References

- [1] Luque, A, Hegedus, S; *Handbook of Photovoltaic Science and Engineering*; John Wiley & Sons, 2003.
- [2] MA Benecke, On the Optical and Electrical Design of LCPV Modules, MSc, Nelson Mandela Metropolitan University, 2012.
- [3] Helmers, H, Bett, AW, Parisi, J and Agert, C; *Modeling of Concentrating Photovoltaic and Thermal systems*; John Wiley & Sons, 2012.
- [4] Incropera, FP, DeWitt, DP; *Fundamentals of heat and mass transfer*; John Wiley & Sons, 2011.
- [5] Jones, AD and Underwood, CP; *A Thermal Model for Photovoltaic Systems*; John Wiley & Sons, 2001.
- [6] Smith, FG, King, TA, Wilkins, D; *Optics and Photonics: An Introduction* (Pages 103-107); 2007.
- [7] Oreski, G, Pinter, G, Knausz, M; *Comparative Study of the Temperature Dependent Delamination Behavior of Four Solar Cell Encapsulants to Glass and Backsheet-laminate*; [s.a.].
- [8] Typical Damages at Solar Panels. 2012. Internet:  
[http://www.europe-solar.de/catalog/index.php?main\\_page=page&id=44](http://www.europe-solar.de/catalog/index.php?main_page=page&id=44) (Accessed: 14 November 2012)
- [9] The Technology of Solar Cells. 2012. Internet:  
<http://cubesat.wikidot.com/the-technology-of-solar-cells> (Accessed: 20 November 2012)

## **Chapter 6**

# **CONCLUSION**

The analysis of the optical-, electrical- and thermal subsystems is essential for the design and implementation of an efficient, economically viable LCPV system. This chapter consolidates the results of chapters 3, 4, and 5 and makes recommendations with regard to the design of LCPV systems in the future.

## 6.1 Optical Sub - System

The 7-facet line-focused reflector system achieved an effective concentration ratio of approximately 4.7. The corresponding geometric concentration is 4.83, which indicates that less than 2.5% of the incoming irradiance is lost through optical imperfections. The effective concentration ratio is also 60% greater than previous V-trough LCPV systems. The concentration ratio may be increased by adding more reflector facets, but an extrapolation of the optical model, as shown in Figure 6.1, suggests that this may not be economically viable. Although an extensive evaluation of the optical sub-system is beyond the scope of this study, the improved concentration ratio and minimal optical losses strongly suggest that the experimental reflector system is an effective method of concentrating sunlight in a LCPV system.

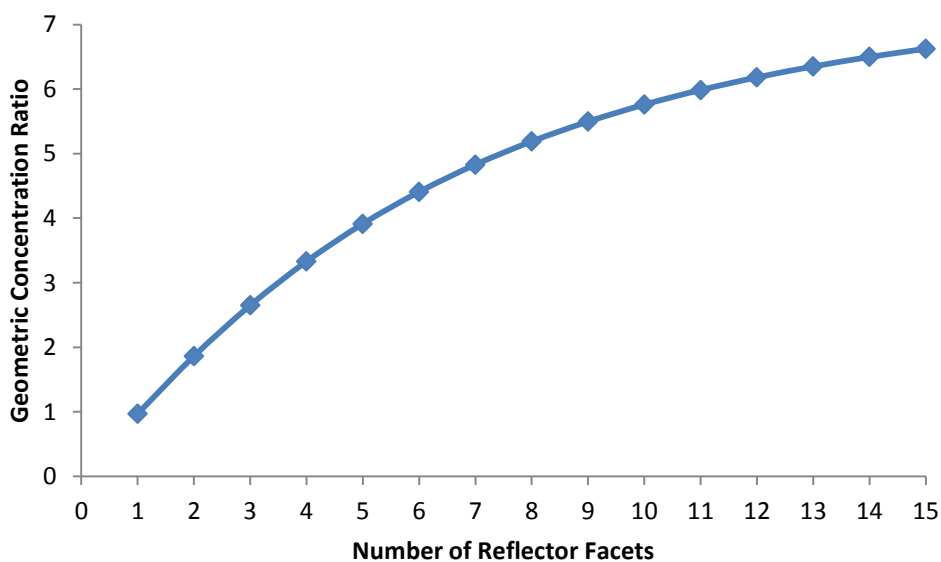


Figure 6.1: Graph showing geometric concentration ratio as a function of number of facets

## 6.2 Electrical Sub - System

Simulated I-V curves, based on the 1-diode model, showed that series resistance significantly contributes to power losses in a LCPV system. The simulated fill factor of a PV cell, with a series resistance of  $0.05\Omega$ , decreased from 0.75 under 1X concentration to 0.44 under 3X concentration conditions, which corresponds to a power loss of more than 40% under concentration. Figure 6.2 shows simulated I-V curves corresponding to a series resistance of  $0.05\Omega$ . However, power losses can be minimized by decreasing the size of the PV cell and subsequently decreasing the short circuit current. By halving the size of the PV cell, the simulated maximum power point increased by approximately 20%.

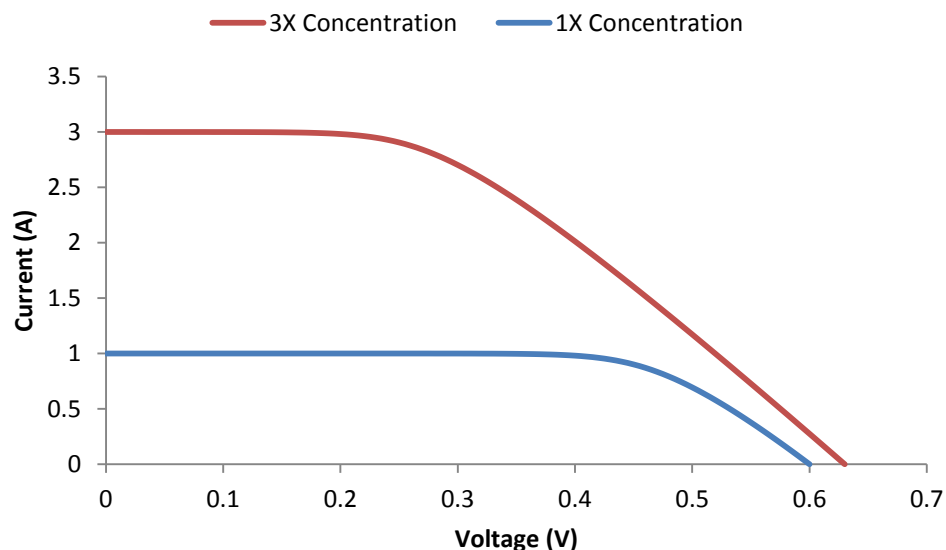


Figure 6.2: I-V characteristic showing the effect of series resistance under concentration

Three PV receivers, consisting of 4-, 6- and 8 cells, were manufactured. The short circuit current, open circuit voltage, maximum power point and fill factor of each PV receiver are listed in Table 6.1. Under concentration, the 8-cell PV receiver achieved a maximum power point of 7.13W, which corresponds to a 23% improvement compared to the 4-cell PV receiver. However, the maximum power point is relatively unchanged under 1-sun conditions. Experimentally, resistive losses are thus not significant under 1-sun conditions, but the increased short circuit current associated with concentration significantly amplifies the effect of series resistance. Figure 6.3 shows the I-V curve of each PV receiver under concentration.

Table 6.1: I-V parameters of the 4-, 6- and 8-cell receivers

	4-Cell	
	1-Sun	4.83-Sun
$I_{sc}$	1.13 A	5.28 A
$V_{oc}$	2.28 V	2.43 V
$P_{max}$	1.62 W	5.78 W
	6-Cell	
	1-Sun	4.83-Sun
$I_{sc}$	0.72 A	3.38 A
$V_{oc}$	3.51 V	3.61 V
$P_{max}$	1.48 W	6.50 W
	8-Cell	
	1-Sun	4.83-Sun
$I_{sc}$	0.54 A	2.56 A
$V_{oc}$	4.73 V	4.88 V
$P_{max}$	1.67 W	7.13 W

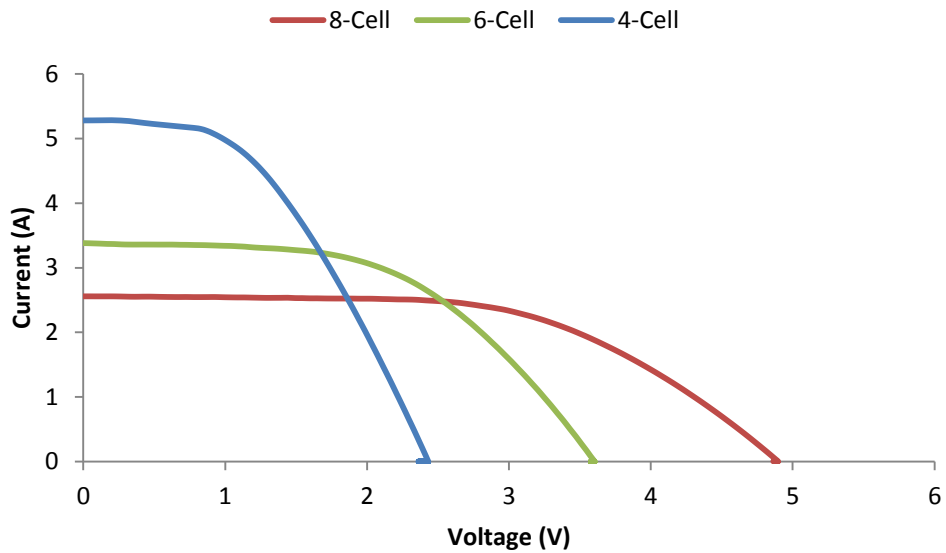


Figure 6.3: I-V characteristics of the 8-, 6- and 4-cell under 4.83-sun conditions at direct irradiance of  $1000\text{W}/\text{m}^2$

### 6.3 Thermal Sub - System

A thermal model, based on an energy balance between irradiance, convection, radiation and electrical work, was developed to predict the operating temperature of a LCPV system under various environmental conditions. The model was experimentally evaluated by monitoring the temperature of the PV receiver and the increase in air temperature across the PV receiver. The total energy dissipated by the PV receiver corresponded to the total energy absorbed within measurement uncertainty, which suggests that the thermal model is an effective method of estimating operating temperatures in a LCPV system. The thermal model can also be used to empirically calculate the convective transfer co-efficient of the LCPV system.

Experimentally, the thermal model accurately predicted the operating temperature of the LCPV system, within experimental error, under changing air velocity and irradiance. Figure 6.4 shows a comparison between the thermal model and the experimental values for various air velocities. The thermal model also correctly predicted a decrease in operating temperature when electrical work was extracted. In addition, the experimental data indicates that the convective transfer co-efficient is proportional to  $v^{0.55}$ , where  $v$  is the air velocity. This result corresponds closely to the theoretical proportionality of  $v^{0.5}$  for a horizontal plate.

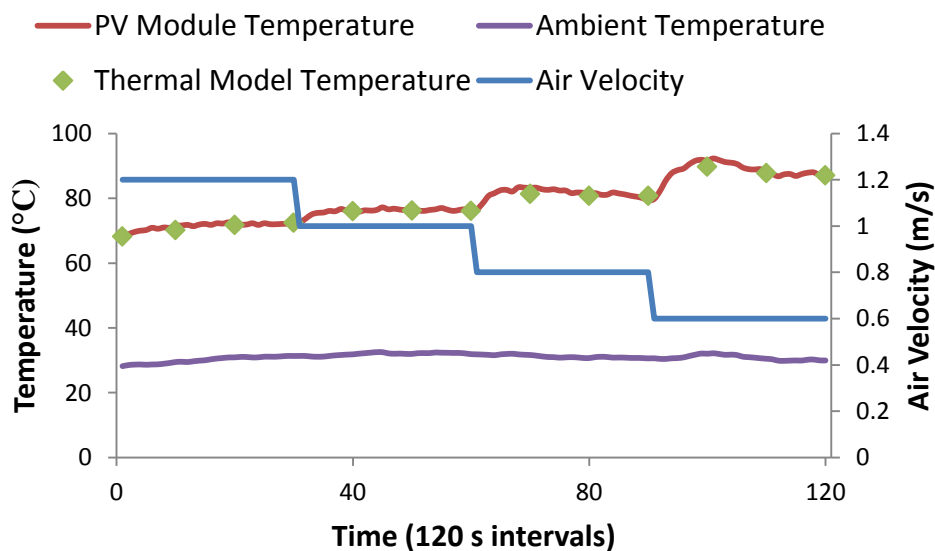


Figure 6.4: Graph showing the dependence of PV receiver temperature on air velocity

A heat sink attached to the PV receiver reduced the temperature difference by a factor of 1.6, but theoretically a factor of 2.35 was expected. It is probable that the fin design of the heat sink decreased the air velocity and subsequently less energy was dissipated through convection. A thermal stress test was also performed to evaluate PV cell degradation under high operating temperature conditions. The PV receiver was subjected to temperatures of above 90°C for more than 25 hours, but no significant change in the I-V characteristic was observed, which indicates that high operating temperatures do not degrade the PV cells used in this study. Figure 6.5 shows the I-V characteristic of the 6-cell PV receiver before and after the thermal stress test.

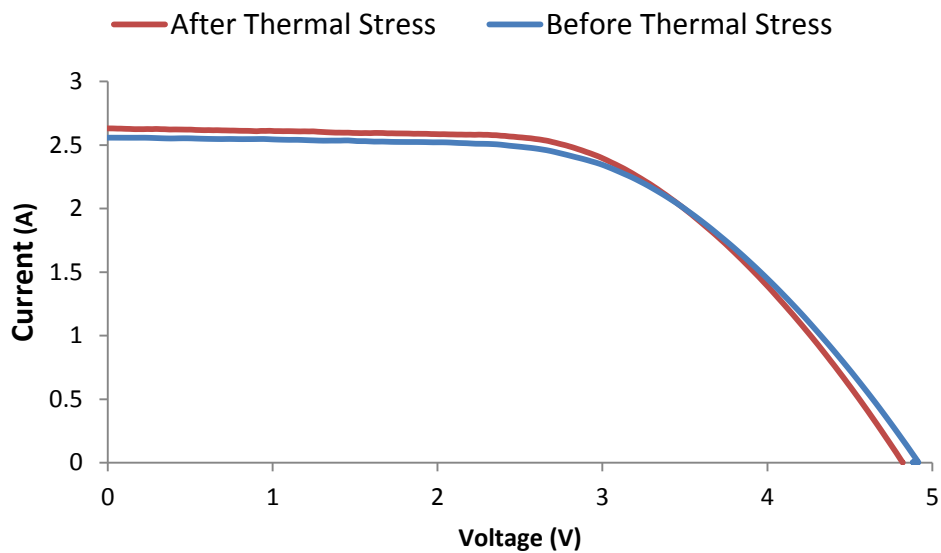


Figure 6.5: IV characteristics of the PV receiver under concentration conditions before/after thermal stress

## 6.4 Recommendations

The 7-facet reflector system had a geometric- and effective concentration ratio of 4.83 and 4.7 respectively. Optical losses are thus less than 2.5%, indicating a satisfactory optical sub-system design. The low current 8-cell PV receiver achieved the highest maximum power point of 7.13W relative to the higher current 6- and 4-cell PV receivers. This suggests that the electrical sub-system can be optimized through the use of small, low current PV cells. The thermal model accurately predicted LCPV operating temperatures under various conditions. The inclusion of a heat sink in the thermal sub-system reduced the operating temperatures, but the results of the thermal stress test suggest that high operating temperatures will not degrade the PV cells.

In accordance with the results of this study, the following recommendations are made with respect to LCPV system design:

- A faceted reflector system, consisting of up to 10 facets, should be used to achieve a satisfactory effective concentration ratio (~5).
- Small, low current PV cells should be used to minimize the effect of series resistance, and maximize the power output.
- An appropriate heat sink should be used to decrease the operating temperature, and consequently increase the maximum power point.

## Appendix: Mathematica Code

```
cl=Input["PV receiver length"];
nd=Input["PV receiver height"];
nf=Input["Number of facets"];
x=c;
y=0;

For[i=1,i<=nf,i++,
theta=N[ArcTan[x/nd]]/2;
x1=Cos[theta]*(cl*Sin[(Pi/2)-(2*theta)])/Sin[(Pi/2)+theta];
r=(cl*Sin[(Pi/2)-(2*theta)])/Sin[(Pi/2)+theta];
x=x+x1;
y=x1*Tan[theta];
nd=nd-y;
Print[x," ",y," ",nd," ",theta/(2*Pi)*360," ",r]
]
```